

7

**ELECTROMAGNETIC BACKSCATTERING FROM
PENETRABLE ROUGH SURFACES BASED ON MOMENT METHOD**

by

VINCENT THOMASSIER

Engineer of Polytechnic School, August 1995

Palaiseau, France

Submitted to the Department of
Electrical Engineering and Computer Science
in Partial Fulfillment of the Requirements for the Degree of

MASTER OF SCIENCE IN ELECTRICAL ENGINEERING


at

MASSACHUSETTS INSTITUTE OF TECHNOLOGY

September 1997

©1997 Massachusetts Institute of Technology
All rights reserved

Signature of Author



Department of Electrical Engineering and Computer Science
August 1st, 1997

Certified by



Professor Jin Au Kong
Professor of Electrical Engineering
Thesis Supervisor

Certified by



Dr. Kung Hau Ding
Research Scientist
Thesis Supervisor

Accepted by



Arthur C. Smith
Chairman, Committee on Graduate Students
Department of Electrical Engineering and Computer Science

**ELECTROMAGNETIC BACKSCATTERING
FROM PENETRABLE ROUGH SURFACES
BASED ON MOMENT METHOD**

by

VINCENT THOMASSIER

Submitted to the Department of
Electrical Engineering and Computer Science
on August 1st, 1997 in Partial Fulfillment of the
Requirements for the Degree of Master of Science in
Electrical Engineering

ABSTRACT

The problem of electromagnetic wave scattering by rough surfaces is of great interest in many fields of applied science and engineering, such as the microwave remote sensing of ocean surface and geophysical terrain. Different numerical approaches have been used in the remote sensing community to compute electromagnetic scattering from random rough surfaces, but their use is limited since they are highly computational intensive. In order to minimize the computational time, this thesis investigates the key parameters required by the Method of Moments (MOM) in solving the backscattering from random rough surfaces. One-scale profiles using the commonly used Gaussian correlation function are compared to profiles with an exponential correlation function, known to be a more realistic description of natural surfaces.

A review of the analytical rough surface scattering theories, as well as the numerical approaches is first given. Three classic analytical theories, Small Perturbation Method (SPM), Physical Optics (PO) approximation and Geometrical Optics (GO) approximation, are applied to derive the backscattering coefficients from a one-dimensional random rough penetrable surface, for both Gaussian and exponential profiles.

The use of Method of Moments to the rough surface scattering is also presented and applied to the problem of a tapered electromagnetic incident wave impinging upon a penetrable profile of finite length. A point-matching approach is used to convert the integral equations in a matrix equation. The matrix equation is then solved using a fast algorithm called Banded Matrix Iterative Approach (BMIA). Ensemble averaging is carried

out in the Monte-Carlo simulations that solve the backscattering coefficients numerically. Gaussian and exponential profiles are generated by a Moving Average Process.

The effects of numerical parameters such as the length of profile, shape of the incident wave, BMIA bandwidth, and the number of unknowns per wavelength, on the convergence process are investigated. This sensitivity study is given both for TE and TM cases, and for different relative dielectric constants. Excellent agreements (less than 0.5 dB) are found between Method of Moments solutions and analytical models within their respective domain of validity. A number of 10 unknowns per wavelength is found to be satisfactory in all cases considered. The length of the profile, as well as the BMIA bandwidth chosen to perform the numerical simulations increase with the correlation length of the surfaces considered. Because of their finest scale-roughness, exponential profiles require longer profiles or more realizations than Gaussian profiles, and are therefore more exigent in computational time. The results depend neither on the polarization nor on the relative dielectric constant of the surface.

Thesis Supervisor: Professor Jin Au Kong
Title: Professor of Electrical Engineering

Thesis Supervisor: Dr. Kung Hau Ding
Title: Research Scientist

ACKNOWLEDGMENTS

I would like to thank first and foremost, my thesis advisors, Professor Jin Au Kong and Dr. Kung Hau Ding. I am grateful for having had the opportunity and the honor to be a part of Professor Kong's famous research group. I will always remember Professor Kong's human qualities that make him the best teacher I have ever known. I thank Dr. Kung Hau Ding for his endless patience. Without his numerous advises, his support and corrections, this thesis will certainly not have been completed.

I would like to thank Dr. Le Toan and Jean-Claude Souyris from CESBIO, as well as Francesco Matera from ITIS-CNR, who were closely involved in this work.

Thanks to Dr. Eric Yang for his maintenance and help on the computer network. It has been a pleasure to know and work with Yan Zhang, who helped me throughout these months to discover and fix many theoretical problems. I am grateful for having met such outstanding students as Li-Fang Wang, Shih-En Shih, Chi On Ao and Makkalon Em. I wish to have a special thought to Kit Wah Lai, who was the "smile" of this group.

These acknowledgments would not be completed without specially thanking Jerry Akerson. Our almost daily coffee-breaks made me discover an awesome human being, and hopefully a friend.

I wish to thank the Delegation Generale de l'Armement that provided the financial support to follow this program at MIT.

Finally, I wish to express my love and gratitude to my wonderful wife Diane-Aurore, who has been so patient and caring during this stressful year. I certainly will not be here today if not for you. Merci.

To Diane-Aurore and our baby

Table of Contents

Acknowledgments	4
Dedication	5
Table of Contents	6
List of Figures	9
List of Tables	12
1. Introduction	14
1.1. Background and Motivation.....	14
1.2. Standard Methods	15
1.2.1. Direct Methods.....	15
1.2.2. Indirect Methods.....	17
1.3. Active Remote Sensing Method.....	20
1.3.1. Radar Equation.....	20
1.3.2. Application to the Remote Sensing of Soil Moisture	21

1.4. Analytical Rough Surface Scattering Models.....	22
1.5. Numerical Methods.....	24
1.5.1. Method of Moments.....	24
1.5.2. Matrix Inversion Methods	28
1.6. Overview of Thesis.....	28
2. Backscattering by a Random Profile Solved using Method of Moments	30
2.1. Integral Equation Formulation	30
2.2. Conversion of the Integral Equation to Matrix Equation.....	34
2.3. Banded Matrix Iterative Approach.....	38
2.4. Scattered Field	40
2.5. Backscattering Coefficient.....	41
3. Analytical Rough Surface Scattering Models	44
3.1. Small Perturbation Method	44
3.2. Physical Optics Approximation	46
3.3. Geometrical Optics Approximation.....	48
4. Numerical Simulation and Comparison	50
4.1. Profile Generators	51
4.2. Simulations and Results	57

4.2.1. Small Perturbation Method	57
4.2.2. Physical Optics Approximation	67
4.2.3. Geometrical Optics Approximation.....	79
5. Summary	86
Appendix	89
Summary	91

List of Figures

Figure 1.1. Geometry of electromagnetic wave scattering from a rough surface profile.	26
Figure 2.1. Geometry of the electromagnetic scattering problem for TE case.	31
Figure 4.1. (a) Gaussian, (b) Exponential Profile.....	53
Figure 4.2. Correlation function of a generated Gaussian profile compared to the theoretical correlation function.....	55
Figure 4.3. Correlation function of a generated exponential profile compared to the theoretical correlation function.....	56
Figure 4.4. TE case: Study of convergence as a function of the number of realizations for an exponential profile with $L=80\lambda$, $kl=1.396$, $k\sigma=0.035$, and $\epsilon_2=(3,0.1)$...	59
Figure 4.5. TE case: Study of convergence as a function of the length of surface for an exponential profile with $kl=1.396$, $k\sigma=0.035$, and $\epsilon_2=(3,0.1)$	60
Figure 4.6. TE case: Comparison between MOM results and Small Perturbation Method model for an exponential profile of $kl=1.396$, $k\sigma=0.035$, and $\epsilon_2=(3,0.1)$.	63
Figure 4.7. TE case: Study of convergence in function of the number of realizations for a Gaussian profile with $L=20\lambda$, $kl=1.396$, $k\sigma=0.035$, and $\epsilon_2=(3,0.1)$	64

Figure 4.8. TE case: Comparison between MOM results and Small Perturbation
Method model for a Gaussian profile of $kl = 1.396$, $k\sigma = 0.035$, and $\epsilon_2 = (3,0.1)$... 65

Figure 4.9. TM case: Comparison between MOM results and Small Perturbation
Method model for a Gaussian profile of $kl = 1.396$, $k\sigma = 0.035$, and $\epsilon_2 = (3,0.1)$... 68

Figure 4.10. TM case: Comparison between MOM results and Small Perturbation
Method model for an exponential profile of $kl = 1.396$, $k\sigma = 0.035$, and $\epsilon_2 = (3,0.1)$. 69

Figure 4.11. TE case: Comparison between MOM results and Small Perturbation
Method model for a Gaussian profile of $kl = 1.396$, $k\sigma = 0.035$, and $\epsilon_2 = (9,1)$ 70

Figure 4.12. TE case: Comparison between MOM results and Small Perturbation
Method model for an exponential profile of $kl = 1.396$, $k\sigma = 0.035$, and $\epsilon_2 = (9,1)$. 71

Figure 4.13. TE case: Study of convergence as a function of the length of the profile
and the number of realizations for an exponential profile of $kl = 8.29$, $k\sigma = 0.62$, and
 $\epsilon_2 = (3,0.1)$ 73

Figure 4.14. TE case: Study of convergence for $L=40\lambda$ and $L=80\lambda$ for an
exponential profile of $kl = 8.29$, $k\sigma = 0.62$, and $\epsilon_2 = (3,0.1)$ 74

Figure 4.15. TE case: Comparison between MOM results and Physical Optics Model
for an exponential profile of $kl = 8.29$, $k\sigma = 0.62$, and $\epsilon_2 = (3,0.1)$ 75

Figure 4.16. TE case: Comparison between MOM results and Physical Optics model
for a Gaussian profile of $kl = 8.29$, $k\sigma = 0.62$, and $\epsilon_2 = (3,0.1)$ 78

Figure 4.17. TE case: Comparison between MOM results and Physical Optics model
for a Gaussian profile of $kl = 8.29$, $k\sigma = 0.62$, and $\epsilon_2 = (9,1)$ 80

Figure 4.18. TE case: Comparison between MOM results and Physical Optics model for an exponential profile of $kl = 8.29$, $k\sigma = 0.62$, and $\epsilon_2 = (9,1)$ 81

Figure 4.19. Comparison between MOM results and Geometrical Optics model for a Gaussian profile of $kl = 17.9$, $k\sigma = 5.95$, and $\epsilon_2 = (3,0.1)$ 84

List of Tables

Table 4.1.1. Moving Average in Gaussian and exponential case.....	52
Table 4.2.1. Frequency and statistical parameters of the profile.....	58
Table 4.2.2. Parameters used for the numerical simulations for Gaussian case.....	61
Table 4.2.3. Estimated surface statistical parameters.	62
Table 4.2.4. TE backscattering coefficients of the MOM and the analytical SPM method for the exponential correlation function case.	62
Table 4.2.5. Estimated surface statistical parameters.	65
Table 4.2.6. TE backscattering coefficient of the MOM and of the analytical SPM method for the Gaussian correlation function case.	65
Table 4.2.7. Frequency and statistical parameters of the profile.....	67
Table 4.2.8. Parameters used for numerical simulations for exponential case.....	72
Table 4.2.9. Estimated surface statistical parameters.	75
Table 4.2.10. TE backscattering coefficients of the MOM and the analytical PO method for the exponential correlation function case.	75
Table 4.2.11. Parameters used for numerical simulations for Gaussian case.....	77

Table 4.2.12. Estimated surface statistical parameters.....	77
Table 4.2.13. TE backscattering coefficients of the MOM and the PO analytical method for the Gaussian case.	77
Table 4.2.14. Frequency and statistical parameters of the profile.	82
Table 4.2.15. Parameters used for the numerical simulations for the Gaussian case. .	83
Table 4.2.16. TE backscattering coefficients of the MOM and the analytical GO method for the Gaussian case.	83

Chapter 1

Introduction

1.1. Background and Motivation

The problem of electromagnetic wave scattering from random rough surfaces is a problem of interest in many different fields of applied physics, such as the remote sensing of ocean surface or earth terrain [1-3]. For instance, the backscattering coefficients measured by electromagnetic sensors have been used to determine the volumetric moisture content of soil [3]. The advantage appeared to be considerable. This air-borne or space-borne method allowed quick and periodical measurements on large areas, which was impossible to perform with classical methods. In Sections 1.1 and 1.2, a general survey of some classical method of measurements of soil moisture will be presented to outline the importance of remote sensing techniques.

This soil moisture is an important parameter in such different areas as agriculture, hydrology and meteorology [4]. In agriculture, the growth of vegetation, cultivated crops, range and forest, is related to soil moisture. Drought or excessive moisture deviations from optimum levels will reduce immediate and future yields. In hydrology, there are several factors pertaining to the hydrologic cycle that are related to soil moisture. For climate and weather forecasting, the ability of soil to store and release water through evapotranspiration

is an important parameter. The temporal variations of soil moisture are then used in flux studies.

These numerous applications lead the remote sensing community to develop inversion models to retrieve this crucial information from the measurement of backscattering coefficients. In Sections 1.3 to 1.4, a review of the existing numerical and analytical rough surface scattering models will be made.

1.2. Standard Methods

1.2.1. Direct Methods

The determination of water content may be accomplished by measuring the amount of water removed from a given sample by evaporation or chemical reaction. Measurements based on the gravimetric method involves weighting a wet sample before and after the water is removed. The water content is then equal to the difference between the masses of the wet and dry samples, divided by the mass of the dry soil. The ratio S is obtained as [6]

$$S = (\text{mass of wet sample} - \text{mass of dry sample}) / \text{mass of dry sample} \quad (1.1)$$

where the soil moisture is then expressed on a weight basis (g/100 g studied). Water content may be removed in different ways, but oven drying the sample at 105°C is the most common method. However, this temperature seems to have been chosen without adequate consideration of the drying characteristics of soil.

The main problem of the above method is the wide variability of results depending on the definition of this "dry" state. In most of the procedures used, the "dry" state is defined when the sample reaches a constant weight. Hence, to obtain accurate and reproducible water content measurements, the sample must be dried at a specified temperature to

constant weight with nothing being lost but water. Unfortunately, soil is not a homogenous medium. It is made of organic materials, colloidal and non-colloidal mineral particles, volatile liquids, chemical substances dissolved in water, and, of course, water. Hence, after having dried the sample, there is no certitude that the loss of weight was only due to the removed water.

The case of the colloidal fraction is complicated since the water present in these particles may either be structural water or adsorbed water. The term "structural water" refers to water that is part of the mineral lattice itself, and "adsorbed water" is water attached to this lattice [6]. It is very difficult to tell them apart in most of the cases. Moisture content is a function of adsorbed water not structural water. According to Nutting [5], it is always possible to find a range of temperatures where the loss of weight due to the structural water is low. According to Black [6], the range between 165°C and 175°C should give more accurate results.

The problem of defining a dry condition for the organic fraction of a soil is even more difficult. Indeed, this fraction is composed of volatile liquids, undecomposed fragments such as roots, and resistant decomposition products such as polysaccharides or polyuronides. If the temperature is higher than 50°C, these organic materials will be decomposed or oxidized. Since the drying temperature used is over 100°C, decomposition and oxidation should be expected and taken into account when reporting data. Furthermore, when precise measurements are required, precautions must be taken to insure that all samples are dried under the same conditions.

Hence accuracy in determining water content using the standard method depends on the mineral and organic composition of the soil, and on a very subjective definition of a dry state. The time needed to reach constant weight depends on the size of the sample, the size of the oven, and the nature of the soil. The standard procedure advises a drying time of between 10 and 24 hours to reach a relative dry state, and many investigators often observe

weight loss over periods from days to weeks. The oven drying method cannot be used, then, when measurements are required on a hourly basis, as in most agricultural or hydrological applications.

In addition to being time consuming, this method is destructive, requiring that each sample be taken from a different place in the soil under study. This may increase the possibility that a change in water content with position in the sampling area may be interpreted falsely as a change with time, at a particular location.

1.2.2. Indirect Methods

The lack of reliability, the time required, and the destructive sampling of the oven drying method have led researchers to develop indirect methods. These methods allow frequent or continuous measurements. Certain physical or chemical properties of the soil vary with water content. The indirect methods measure these variations and relate them to the water content. Numerous techniques have been devised for measuring soil moisture such as gamma-ray attenuation [7], neutron scattering [7], thermal conductance [6], electrical capacitance [6] and ultrasonic energy [6]. Of these, the first two have gained the greatest acceptance, according to Collet [8].

a. Neutron scattering

The neutron scattering method uses the property of the hydrogen nuclei for scattering and slowing neutrons. Neutrons with high energy (0.1 to 10 Mev) emitted from a radioactive substance such as radium-beryllium are slowed down and scattered by atomic nuclei. This process is called "thermalization", the energy lost by the neutrons becomes the thermal energy of atoms in substance at room temperature. The two key factors involved in this thermalization are the transfer of energy at each collision, and the statistical probability of collision. Since hydrogen nuclei are of the same size and mass as neutrons, they have a greater thermalizing effect than most of the other elements such that they are qualified as

efficient "thermalizers". Therefore, the slow neutron count provides a measure of the hydrogen content of the soil and then of the water [7].

The nature of the thermalization process and neutron scattering implies important restrictions on the resolution of the measurements. For example, experimental work with radium-beryllium sources indicates that the practical resolution at best is 15 cm; i.e., the volume of soil affecting the neutrons scattering is a sphere of 15 cm in diameter. Furthermore, this resolution decreases when the water content decreases. Hence, at lower water content, the diameter of this sphere increases to 60 cm. This lack of resolution will then prevent us from measuring strong variations or any discontinuities in water content inside this volume. Another limitation is due to the presence in the soil of other nuclei with as efficient thermalization characteristics as hydrogen, such as cadmium, beryllium, lithium, or chlorine. Their presence may lead to erroneous estimations of the amount of hydrogen, and then of the water content.

b. Gamma-ray attenuation

The degree to which an energetic beam is attenuated depends upon the overall density of the soil. If the density of the soil less its water content is constant, variations of attenuation between a dry soil and a wet soil represent changes in the water content. The difference between gamma-ray and neutron scattering methods differ in the way each measures the amount of hydrogen. The gamma-ray attenuation uses the ratio of the transmitted to incident flux for a column of wet soil and the same ratio for the dry soil.

The attenuation equation for the wet soil is given by [7]

$$\frac{N_m}{N_o} = \exp[-S(m_s r_s + m_w Q) - 2S' m_c r_c] \quad (1.2)$$

where

N_m = transmitted flux,

N_o = incident flux,

m_s, m_w, m_c = attenuation coefficient for the soil, water, and container material, respectively

Q = mass of water per unit bulk volume of the soil,

r_s = density of the soil,

r_c = density of the container wall,

S' = thickness of the container wall,

S = thickness of the column of soil.

The corresponding equation for the dry soil is

$$\frac{N_d}{N_o} = \exp[-Sm_s r_s - 2S' m_c r_c] \quad (1.3)$$

where N_d is the transmitted flux for the dry soil case. The ratio of these two measures will provide the mass of water per unit bulk volume of the soil, Q .

The gamma-ray attenuation method requires expensive equipment and cannot be applied directly in the field, but only in a laboratory. Even if it provides unequalled accuracy in the measurements, the complexity of this method make it impracticable for general use.

Even if the precision of soil moisture measurements increased by using indirect methods, such as neutron scattering or gamma-ray attenuation, none of them can provide frequent or continuous measurements on a large field of study. Remote sensing methods from aircraft or satellite appear then to be a solution to this problem.

1.3. Active Remote Sensing Method

1.3.1. Radar Equation

The key equation in active remote sensing is the radar equation that relates the output of the radar to the properties of the target. Any electromagnetic wave sent by radar is indeed reflected by the surface under view. If we assume that the receiver and the transmitter are in the same location, the received power P_r of polarization r is then given by [9]

$$P_r = \frac{P_t G_t^2 \lambda^2 A}{(4\pi)^3 R^4} \sigma_r^o \quad (1.4)$$

where

P_t = transmitted power at polarization t (W),

G_t = gain of the transmitting antenna in the direction of the target at polarization t ,

A = area of the cell illuminated by the transmitted antenna pattern (m^2),

R = distance between radar and target (m),

λ = wavelength (m),

σ_r^o = backscattering radar cross-section describing the target.

The design of the radar is such that P_t , G_t , λ and R normally remain constant or are known during use of the radar. Therefore, the received power characterized by the response of the target varies only with σ_r^o .

The radar cross-section σ_r^o is generally a function of radar parameters, such as the incident angle θ_i , and wavelength λ , and a function of the geometric and electromagnetic properties of the target, ξ , such as shape, conductivity and dielectric constant. Hence, by measuring the variation of these coefficients, we may deduce the properties of the target.

1.3.2. Application to the Remote Sensing of Soil Moisture

For a natural surface, the backscattering cross section is governed by its geometrical properties and its dielectric constant ϵ_r . Moreover, this dielectric property is strongly dependent on the volumetric soil moisture content, mainly because of the large dielectric contrast between dry soil (typically equal to 2-3) and water (approximately equal to 80). Hence, the use of electromagnetic active sensors to retrieve the soil moisture content appeared theoretically logical, and the first experiments done by NASA in June 1970 confirmed this assumption [10]. During the flight, several fields were observed by the scatterometer, which observed sharp change as it flew between irrigated and dry sections.

As mentioned above, σ_{rt}^o depends on both the geometrical properties of the illuminated area and its dielectric constant. Generally, it can be expressed as,

$$\sigma_{rt}^o = f[\epsilon_r, \xi] \quad (1.5)$$

when all the other parameters constitutive of radar equation are fixed. The retrieval of soil moisture can be achieved by using scattering models that estimate the backscattering coefficient as a function of the characteristic parameters of a given natural soil surface.

The modeling approach is generally a two-step process. The first step consists of describing the dielectric properties and the roughness characteristics of the soil surface. In the past, several models were developed to relate the dielectric constant to soil parameters. De Loor [11], Hoekstra and Delaney [12] considered a soil-water mixture, whereas Dobson [13] developed a semi-empirical model for a four component mixture (soil solid, air, free water, and bound water). However, the most widely used for non saline soil moisture is the empirical model of Hallikainen [14], which gives the dielectric constant as a function of volumetric soil moisture and soil texture (percentage of sand, loam and clay). This model will be used throughout this work. The roughness of a natural surface is

generally described by three different models. The first one is a deterministic description, where profiles are characterized by periodic shapes, such as sinusoidal functions. The second model uses a stochastic description to represent the surface as one-scale random rough surfaces. The height distribution is characterized by a Gaussian probability density function, a correlation function in the horizontal direction, often chosen as Gaussian, and the standard deviation, σ , of the height distribution. The third model is a combination of the first two, and has been studied by Shin et al [15]. However, recent studies [16-18] underlined the presence of different scales of roughness for the natural surface, which was not taken into account in these three models. Different attempts have been made to set up more realistic soil surface descriptions. Hence, Church [16] considered a natural surface as the result of random changes affecting an initial surface, and used the multi-layer stacks approach in his model [19]. The fractal approach is an alternative approach to treat this multi-scale effect. This description is well known for vegetation [20], and is also investigated for the geometry of soils [22-23]. The height profile is described by Weierstrass functions as in Jaggard [24].

The second step consists of applying electromagnetic scattering theories to the selected surface description. The objective of the following section is to review the currently existing theories leading to analytical models, as well as their respective range of validity.

1.4. Analytical Rough Surface Scattering Models

Relatively simple analytic solutions exist that have different domains of validity, in terms of roughness conditions. Back in 1951, Rice [25] developed a theory to obtain the polarization dependence of the scattering from slightly rough surfaces, which is in a way similar to the more generalized Small Perturbation Method (SPM). This perturbation theory requires small surface rms height and slopes, with respect to the wavelength. In 1967, Valenzuela extended Rice theory to the second order for the estimation of the

depolarization of electromagnetic waves from slightly rough surfaces [26]. When the surface roughness is such that the correlation length and the radius of curvature are much larger than the wavelength, the basic assumption of the Kirchhoff approximation can be made. The surface is then approximated by a series of small planar facets [3]. This approximation is the basis for two other models, the Physical Optics (PO) and Geometrical Optics (GO), which requires additional simplifications to lead to explicit analytical expressions. The domain of validity of these widely used models have been studied in the past and their analytical definitions are available [3]. These three classical models, SPM, PO and GO, will be considered in this thesis and the backscattering expressions for a one-dimensional penetrable rough surface will be given in Chapter 3. Ishimaru and Chen [27] extended the domain of validity of the Kirchhoff approximation to very rough surfaces with the second order approximation coupled with shadowing effects. In addition to these classical models, the last decade has spawned the two-scale scattering [28-29], the phase perturbation methods [30-32], the momentum transfer expansions [33-34], the full wave theory [35], the magnetic field integral iterations [36], and the Integral Equation Method [37-38].

In spite of the wealth of theories, the regime of application of each theory and its validity domain have not been fully determined. The main reason is the absence of exact solutions for the rough surface scattering problem and the lack of experimental results for comparison. Even with experimental results available, problems of calibration and variations of the local statistics of surfaces make this comparison difficult. These considerations, associated with the increasing computational power of computers, have suggested the comparison of these theoretical approximations with numerical solutions obtained by solving exactly the problem of scattering upon an ensemble of simulated rough surfaces. The following section reviews the numerical approaches developed in the remote sensing community, in particular, the Method of Moments that will be used in this thesis.

1.5. Numerical Methods

In order to validate the analytical approaches, the exact calculation of scattered field from a rough surface, either Perfectly Conducting (PEC) or penetrable, is required. Numerical methods, such as the Method of Moments (MOM) [39] or the Finite Difference Time Domain (FDTD) algorithm of Yee [40], have been developed in the 1960's to solve this problem. Beside these classical methods, there are other approaches including now the finite element, boundary element, multipole, transmission line, and numerous other methods [41]. However, throughout the years MOM has proved to be the most widely used to solve the single frequency surface scattering problem. The first to follow this direction were Axline and Fung [42], and subsequently Fung and his collaborators [43-45]. Contributions to assess the validity of SPM and Kirchhoff theories for Gaussian height correlation function have been made by Thorsos [46], Thorsos and Jackson [47], Soto-Crespo et al [48], and Sanchez-Gil and Nieto-Viesperinas [49]. Broschat et al [50] conducted a similar study for the phase perturbation theory. Rodriguez et al [51] presented a numerical evaluation of the domain of validity of theories, such as SPM, Kirchhoff approximation, two-scale expansion, momentum transfer expansion, and the unified perturbation method. MOM was used in his study to solve the scattering from a PEC Gaussian random surface described by a power law spectrum. The following sections review the derivation of the Method of Moments and give some examples of numerical methods for efficient matrix inversion.

1.5.1. Method of Moments

The problem of simulating the wave scattering from a one-dimensional, random rough surface was first reported in 1978 by Axline and Fung, using the Method of Moments [42]. This method is applied to obtain the numerical solutions of unknown tangential fields on

the given illuminated surface. The scattered field at any observation point can be then easily obtained by applying the Huygen's principle.

The MOM converts an integral equation in the spatial domain into a matrix equation. These integral equations result from the standard dyadic Green's function formulation of Huygen's principle for a semi-infinite half space [2]. For the problem of Figure 1.1, it yields, for the region 1 above the profile,

$$\begin{aligned} \frac{\hat{n} \times \bar{E}_1(\bar{r})}{2} = & \hat{n} \times \bar{E}_{inc}(\bar{r}) + \hat{n} \times \int_{S'} ds \left\{ i\omega\mu_1 \bar{G}_1(\bar{r}, \bar{r}') \cdot [\hat{n}' \times \bar{H}(\bar{r}')] \right. \\ & \left. + \nabla \times \bar{G}_1 \cdot [\hat{n}' \times \bar{E}(\bar{r}')] \right\} \end{aligned} \quad (1.6)$$

$$\begin{aligned} \frac{\hat{n} \times \bar{H}_1(\bar{r})}{2} = & \hat{n} \times \bar{H}_{inc}(\bar{r}) + \hat{n} \times \int_{S'} ds \left\{ -i\omega\epsilon_1 \bar{G}_1(\bar{r}, \bar{r}') \cdot [\hat{n}' \times \bar{E}(\bar{r}')] \right. \\ & \left. + \nabla \times \bar{G}_1 \cdot [\hat{n}' \times \bar{H}(\bar{r}')] \right\} \end{aligned} \quad (1.7)$$

where the integral is performed as a principle value integration along the profile, \bar{G}_1 is the dyadic Green's function of medium 1, and \hat{n} is a unit normal vector to the surface S' . For the region 2, below the surface profile, the integral equations are

$$\begin{aligned} \frac{\hat{n} \times \bar{E}_2(\bar{r})}{2} = & -\hat{n} \times \int_{S'} ds \left\{ -i\omega\mu_2 \bar{G}_2(\bar{r}, \bar{r}') \cdot [\hat{n}' \times \bar{H}(\bar{r}')] \right. \\ & \left. + \nabla \times \bar{G}_2 \cdot [\hat{n}' \times \bar{E}(\bar{r}')] \right\} \end{aligned} \quad (1.8)$$

$$\begin{aligned} \frac{\hat{n} \times \bar{H}_2(\bar{r})}{2} = & -\hat{n} \times \int_{S'} ds \left\{ -i\omega\epsilon_2 \bar{G}_2(\bar{r}, \bar{r}') \cdot [\hat{n}' \times \bar{E}(\bar{r}')] \right. \\ & \left. + \nabla \times \bar{G}_2 \cdot [\hat{n}' \times \bar{H}(\bar{r}')] \right\} \end{aligned} \quad (1.9)$$

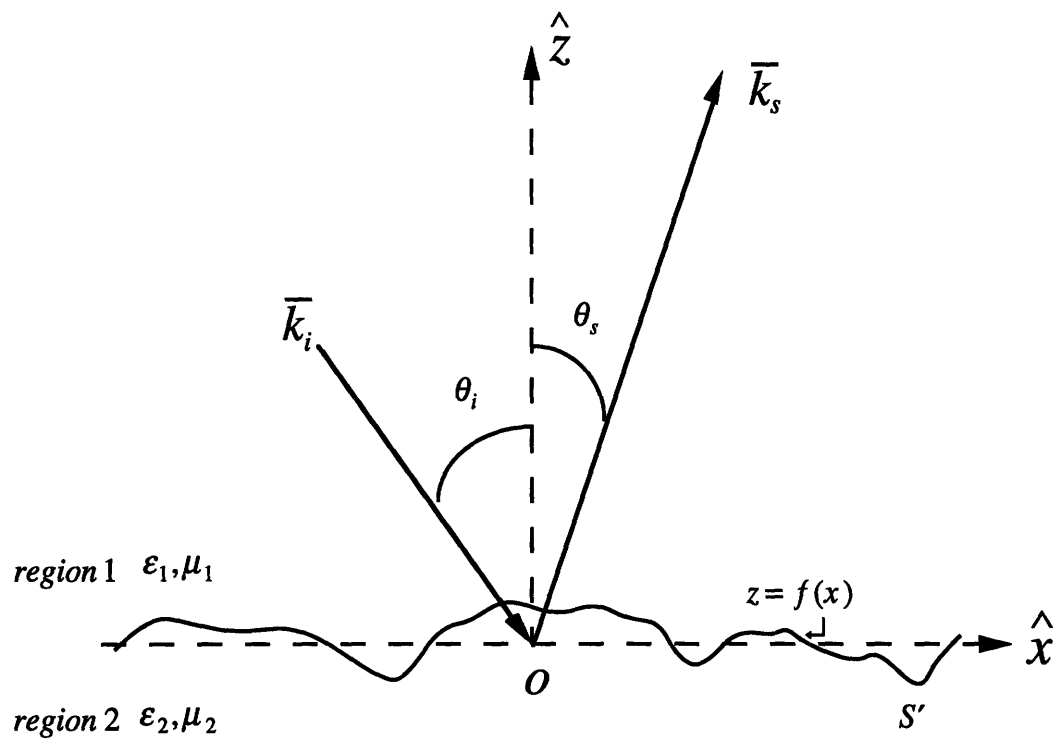


Figure 1.1. Geometry of electromagnetic wave scattering from a rough surface profile.

where $\overline{\overline{G}}_2$ is the dyadic Green's function of medium 2. The continuity of both electric and magnetic tangential fields is implicit in these four equations, since the total fields above and below the profile are created by the same sources. We note that these equations are not independent, and the use of one or combination of (1.6)-(1.7) with one or combination of (1.8)-(1.9) is required to solve this problem. In the Method of Moments, unknown tangential fields are first expanded into a sum of weighted basis functions. These basis functions can be non-zero over a small portion of the domain ("sub domain" functions) or may range over the entire domain ("entire" functions). Exact expansions are limited to very few cases, and higher order solutions are often required to achieve higher accuracy. Among the standard basis functions are pulses (equal to one over a small domain and zero everywhere), triangular (linear over a small domain and zero everywhere) or sinusoidal for "entire" functions. Substitution of these expansions into the integral equation (1.6)-(1.9) converts these equations into summations of integrals over the domain of basis functions.

An inner product is then defined as the multiplication of the integral equations by weighting functions $\overline{\omega}_n(\vec{r})$, followed by an integration over the domain of the weighting functions. These inner products give the following matrix equation,

$$\overline{\overline{Z}}\vec{x} = \overline{V} \quad (1.10)$$

where the vector \overline{V} is given by the inner product of the incident fields with the weighting functions, whereas the elements of the matrix $\overline{\overline{Z}}$ are the results of a double integration over the domains of the weighting and the basis functions. Solutions of this equation will yield the unknown vector \vec{x} , which contains the unknown expansion coefficients of the surface fields. The scattered field at the observation point can be calculated from \vec{x} and Huygen's principle. The use of pulse functions as basis functions together with the delta functions as weighting functions is a technique known as "Point Matching Method" [39].

1.5.2. Matrix Inversion Methods

The limiting factor inherent to this inversion process is the size of the impedance matrix $\bar{\bar{Z}}$. Standard inversion techniques appeared rapidly to be unable to perform efficiently this inversion for long profiles involving thousands of unknowns [53]. The analysis with full matrix inversion was therefore limited to one-dimensional case, that required $O(n^3)$ number of operations, where n is the number of unknowns. For large-scale rough surfaces requiring many unknowns, various iterative algorithms of order n^2 operations were developed to solve this kind of problems. Most of the commonly used iterative approaches are derived from conjugate gradient algorithm [54]. In this thesis, a variant called bi-conjugate gradient-stabilized algorithm (BICGSTAB) will be used. However, these approaches may still be highly computational intensive, depending on the number of iterations required. Since most of the computational time spent was on the multiplication of the matrix with a vector for each iteration, new techniques were therefore developed in recent years to increase the performance of matrix multiplication. The Banded Matrix Iterative Approach (BMIA) [54], or the Sparse Matrix Iterative Approach (SMFSIA) [55] enables us to extend the domain of application of the Method of Moments [56]. This approach will be applied in this thesis in Chapter 2 to solve the integral equations in the case of a one-dimensional penetrable rough surface based on the BMIA method.

1.6. Overview of Thesis

The following thesis is composed of four other parts.

In Chapter 2, the electromagnetic surface scattering problem is solved by using the Method of Moments. The surface is a one-dimensional random rough profile of finite length, characterized by a dielectric constant. The incident TE wave is a Gaussian tapered wave, chosen to avoid edge effects due to the finite length of the profile. The matrix equations are derived, and inverted using the Banded Matrix Iterative Approach (BMIA).

The expression of the backscattering coefficients is based on the Monte-Carlo simulations, which perform the ensemble average numerically.

In Chapter 3, three analytical models, Small Perturbation Method, Physical Optics (PO) and Geometrical Optics (GO) approximation, are described for the one-dimensional case, in their respective domain of validity. The random rough surfaces considered are one-scale surfaces, with Gaussian probability density height distribution, characterized by Gaussian or exponential correlation functions.

In Chapter 4, the numerical results obtained by the MOM are validated through comparisons with the analytical models. A sensitivity study is performed to underline the different numerical requirements for solving electromagnetic scattering from rough surfaces with Gaussian or exponential correlation functions.

Chapter 5 summarizes the work and concludes this thesis.

Chapter 2

Backscattering by a Random Profile Solved using Method of Moments

As underlined in Chapter 1, there are many different approaches to numerically compute the electromagnetic scattering from a one-dimensional profile. For a sinusoidal or periodic profile, a decomposition in Floquet modes of the unknown scattered field is possible, as it has been studied by Chuang and Kong [58] and others [59,60]. Another approach uses a finite length of random rough profile and a tapered incident wave [61,62] where, to avoid edge effects, the incident field falls off slowly near the ends of the surface segment. This approach is applied and described in this chapter to solve the electromagnetic wave scattering from a one-dimensional rough surface problem.

2.1. Integral Equation Formulation

We consider an incident plane wave impinging on a one-dimensional random rough surface, whose profile variation in one direction is given by $z = f(x)$ as shown in Figure 2.1. The plane of incidence is perpendicular to the surface profile. In the one-dimensional case, equations (1.6)-(1.9) can be simplified, since the transversal magnetic and electric fields, H_y and E_y , are sufficient to determine all other field components [63].

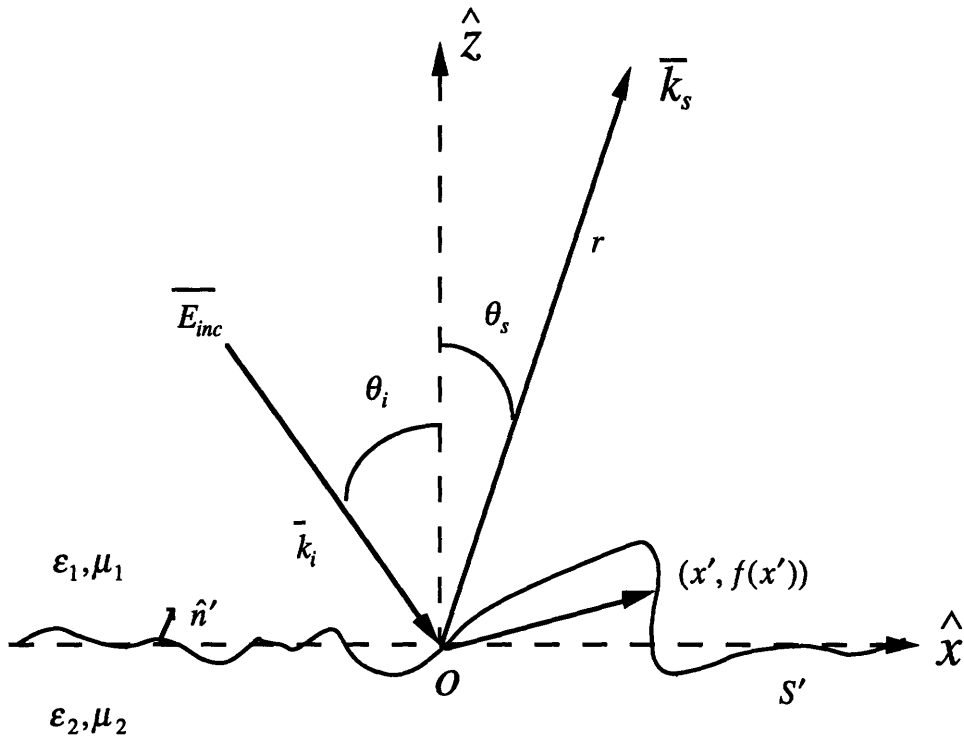


Figure 2.1. Geometry of the electromagnetic scattering problem for TE case.

We thus need to obtain these two field components along the surface profile to fully solve the surface scattering problem. Furthermore, for the incident field impinging upon the profile in the $x - z$ plane, Maxwell's equations can be decomposed into dual equations for both TE and TM fields. Applying the Huygen's principle and the extinction theorem [63] to the regions above and below the surface respectively, we obtain the following, for the TE case,

$$E_{yinc} = \frac{1}{2} E_{y1} - \int_{S'} ds' [E_{y1} \hat{n}' \cdot \nabla_s G_1 - G_1 \hat{n}' \cdot \nabla_s E_{y1}] \quad (2.1)$$

$$0 = \frac{1}{2} E_{y2} + \int_{S'} ds' [E_{y2} \hat{n}' \cdot \nabla_s G_2 - G_2 \hat{n}' \cdot \nabla_s E_{y2}] \quad (2.2)$$

where S' denotes the rough surface on which the surface integration is carried out, $\nabla_s = \hat{x} \frac{\partial}{\partial x'} + \hat{z} \frac{\partial}{\partial z'}$, \hat{n}' is the normal vector to the surface S' , E_{y1} and E_{y2} are respectively the fields above and below the profile, and G_j , ($j=1,2$), is the two-dimensional Green's function for each medium,

$$G_j(\bar{r}, \bar{r}') = \frac{i}{4} H_0^{(1)}(k_j |\bar{r} - \bar{r}'|) \quad (2.3)$$

here $H_0^{(1)}$ is the Hankel function of the first kind and the zeroth order, and $|\bar{r} - \bar{r}'| = \sqrt{(x - x')^2 + (z - z')^2}$.

In equations (2.1)-(2.2), the differential element $ds \hat{n}'$ can be expressed in terms of Cartesian coordinates, as

$$ds \hat{n}' = dx' (\hat{z} - \hat{x} \frac{dz}{dx}) \quad (2.4)$$

The continuity of tangential fields gives the boundary conditions on the surface S' ,

$$E_{y1} = E_{y2} \quad (2.5)$$

$$\frac{\partial E_{y2}}{\partial n'} = \frac{\partial E_{y1}}{\partial n'} \quad (2.6)$$

An incident wave is chosen to be a tapered plane wave as [45]

$$\bar{E}_{inc} = -\hat{y} \exp\left[i\bar{k}_1 \cdot \bar{r}(1 + w(\bar{r})) - (x + z \tan \theta_i)^2 / g^2\right] = -\hat{y} E_{yi} \quad (2.7)$$

where $k_1 = \omega \sqrt{\mu_1 \epsilon_1}$ is the wavenumber of the incident wave, g is the factor controlling the tapering, and

$$w(\bar{r}) = \frac{2(x + z \tan \theta_i)^2 / g^2 - 1}{(k_1 g \sin \theta_i)^2} \quad (2.8)$$

This form of the tapered incident wave has been shown to satisfy the scalar Helmholtz wave equation to the order of $1/(k_1 g \sin \theta_i)^2$ [45].

Similarly for the TM case, the corresponding integral equations for the surface magnetic fields are

$$H_{yinc} = \frac{1}{2} H_{y1} - \int_{S'} ds' \left[H_{y1} \hat{n}' \cdot \nabla_s G_1 - G_1 \hat{n}' \cdot \nabla_s H_{y1} \right] \quad (2.9)$$

$$0 = \frac{1}{2} H_{y2} + \int_{S'} ds' \left[H_{y2} \hat{n}' \cdot \nabla_s G_2 - G_2 \hat{n}' \cdot \nabla_s H_{y2} \right] \quad (2.10)$$

and the boundary conditions are, at the surface,

$$H_{y1} = H_{y2} \quad (2.11)$$

$$\frac{\partial H_{y1}}{\partial n'} = \frac{\epsilon_1}{\epsilon_2} \frac{\partial H_{y2}}{\partial n'} \quad (2.12)$$

The following section derives the matrix equation that is used in the Method of Moments to solve the surface fields , in equations (2.1-2.4).

2.2. Conversion of the Integral Equation to Matrix Equation

The integral equations (2.1)-(2.2) can be converted to a matrix equation using the Point Matching Method [39]. In this method, the unknown function, X , is decomposed using a set of basis functions, $(f_n(x))_{n=\{0,1,\dots\}}$, such that

$$X = \sum_n a_n f_n(x) \quad (2.13)$$

with a_n being the unknown expansion coefficients. The basis functions of the Point Matching Method are chosen as pulses functions $f_n(x)$, defined by

$$f_n(x) = \begin{cases} 1 & \text{for } x \in \left[-\frac{L}{2} + (n-1)\Delta x; -\frac{L}{2} + n\Delta x\right] \\ 0 & \text{elsewhere} \end{cases} \quad (2.14)$$

where the profile S' has been limited between $-L/2$ and $L/2$, and discretized into N subsegments, each of length $\Delta x = L/N$. The inner product is next performed, with weighting functions chosen as delta functions, defined by

$$w_n(x') = \delta(x - x_n) \text{ where } x_n = -L/2 + (n - 1/2)\Delta x, \quad n = 1, 2, 3, \dots, N \quad (2.15)$$

The integral equations (2.1) and (2.2) are thus replaced by sums over the discretized profile as

$$E_{yi}(x_n) = \frac{1}{2} F_1(x_n) + \sum_{m=1}^N [G_1(r_{nm}) F_2(x_m) - F_1(x_m) D_1(r_{nm})] \Delta x \quad (2.16)$$

$$0 = \frac{1}{2} F_1(x_n) - \sum_{m=1}^N [G_2(r_{nm}) F_2(x_m) - F_1(x_m) D_2(r_{nm})] \Delta x \quad (2.17)$$

where $n = 1, 2, 3, \dots, N$,

$$r_{mn} = \sqrt{(x_m - x_n)^2 + (f(x_m) - f(x_n))^2} \quad (2.18)$$

$$G_j(r_{mn}) = \frac{i}{4} H_0^{(1)} \left(k_j \sqrt{(x_m - x_n)^2 + (f(x_m) - f(x_n))^2} \right) \quad (2.19)$$

$$D_j(r_{mn}) = \frac{ik_j}{4r_{mn}} H_0^{(1)} \left(k_j \sqrt{(x_m - x_n)^2 + (f(x_m) - f(x_n))^2} \right) \\ \times (f(x_n) - f(x_m) - f'(x_m)(x_n - x_m)) \quad (2.20)$$

for $j=1, 2$, and

$$F_1(x_m) = E_y(x_m) \quad (2.21)$$

$$F_2(x_m) = \left(\hat{z} - \hat{x} \frac{dz}{dx} \right) \cdot \nabla_s E_y(x_m) \quad (2.22)$$

are the surface unknowns.

As a result, a matrix equation is formed as

$$\bar{\bar{Z}} \bullet \bar{X} = \bar{V} \quad (2.23)$$

where \bar{X} , and \bar{V} are vectors of $2N \times 1$ dimension, whose components are, respectively,

$$X_n = \begin{cases} F_1(x_n) & \text{for } 1 \leq n \leq N \\ F_2(x_n) & \text{for } N+1 \leq n \leq 2N \end{cases} \quad (2.24)$$

and

$$V_n = \begin{cases} E_{yi}(x_n) & \text{for } 1 \leq n \leq N \\ 0 & \text{for } N+1 \leq n \leq 2N \end{cases} \quad (2.25)$$

The impedance matrix, $\bar{\bar{Z}}$, is

$$\bar{\bar{Z}} = \begin{bmatrix} \bar{A} & \bar{B} \\ \bar{C} & \bar{D} \end{bmatrix}. \quad (2.26)$$

with the matrix elements given by

$$A_{mn} = \frac{i\Delta x k_1}{4r_{mn}} H_1^{(1)} \left(k_1 \sqrt{(x_m - x_n)^2 + (f(x_m) - f(x_n))^2} \right) \\ \times (f'(x_m)(x_n - x_m) - f(x_n) - f(x_m)) \quad (2.27)$$

$$B_{mn} = \frac{i\Delta x}{4} H_0^{(1)} \left(k_1 \sqrt{(x_m - x_n)^2 + (f(x_m) - f(x_n))^2} \right) \quad (2.28)$$

$$C_{mn} = -\frac{i\Delta x k_2}{4r_{mn}} H_1^{(1)} \left(k_2 \sqrt{(x_m - x_n)^2 + (f(x_m) - f(x_n))^2} \right) \\ \times (f'(x_m)(x_n - x_m) - f(x_n) - f(x_m)) \quad (2.29)$$

$$D_{mn} = \frac{i\Delta x}{4} H_0^{(1)} \left(k_2 \sqrt{(x_m - x_n)^2 + (f(x_m) - f(x_n))^2} \right) \quad (2.30)$$

where $f'(x)$ is the first derivative of $f(x)$. It is noted that in the TM case, the matrix elements D_{mn} become

$$D_{mn} = \frac{i\Delta x \varepsilon_2}{4 \varepsilon_1} H_0^{(1)} \left(k_2 \sqrt{(x_m - x_n)^2 + (f(x_m) - f(x_n))^2} \right) \quad (2.31)$$

The diagonal elements need particular attention and are obtained by using the small argument approximation for both $H_0^{(1)}$ and $H_1^{(1)}$, the Hankel functions of the first kind, of the zeroth and first order respectively, [2]

$$H_0^{(1)}(k\rho) \approx 1 - i \frac{2}{\pi} \ln \left[\frac{2}{\gamma k \rho} \right] \text{ when } k\rho \ll 1 \quad (2.32)$$

$$H_1^{(1)}(k\rho) \approx -i \frac{2}{\pi k \rho} \text{ when } k\rho \ll 1 \quad (2.33)$$

with $e = \exp(1)$, $\ln \gamma = 0.5772156649$, and $\gamma_n = \sqrt{(1 + f'(x_n)^2)}$. Thus, we have for the diagonal elements,

$$A_{nn} = \frac{1}{2} - \frac{f''(x_n)\Delta x}{4\pi \gamma_n^2} \quad (2.34)$$

$$B_{nn} = \frac{i\Delta x}{4} H_0^{(1)} \left(\frac{k_1 \Delta x \gamma_n}{2e} \right) \approx \frac{i\Delta x}{4} \left(1 - i \frac{2}{\pi} \ln \left[\frac{4e}{\gamma k_1 \Delta x \gamma_n} \right] \right) \quad (2.35)$$

$$C_{nn} = \frac{1}{2} + \frac{f''(x_n)\Delta x}{4\pi \gamma_n^2} \quad (2.36)$$

$$D_{nn} \approx -\frac{i\Delta x}{4} H_0^{(1)}\left(\frac{k_2 \Delta x \gamma_n}{2e}\right) \approx -\frac{i\Delta x}{4} \left(1 - i\frac{2}{\pi} \ln\left[\frac{4e}{\gamma k_2 \Delta x \gamma_n}\right]\right) \quad (2.37)$$

The following section presents the numerical method, BMIA, used to perform efficiently the matrix inversion.

2.3. Banded Matrix Iterative Approach

The evaluation of the unknowns \bar{X} in (2.23) is obtained by using the Banded Matrix Iterative Approach (BMIA) that is much more computationally efficient and faster than an exact matrix inversion technique [54,56].

In the BMIA method, the two sets of unknowns F_1 and F_2 are first labeled alternatively in a new unknown vector \bar{X}_{BMIA} defined as

$$\bar{X}_{BMIA} = \begin{bmatrix} F_1(x_1) \\ F_2(x_1) \\ F_1(x_2) \\ F_2(x_2) \\ \cdot \\ \cdot \\ \cdot \\ F_2(x_N) \end{bmatrix} \quad (2.38)$$

Thus the corresponding matrix equation becomes

$$\bar{Z}_{BMIA} \cdot \bar{X}_{BMIA} = \bar{V}_{BMIA} \quad (2.39)$$

where

$$\bar{V}_{BMA} = \begin{bmatrix} E_{yi}(x_1) \\ 0 \\ E_{yi}(x_2) \\ 0 \\ \cdot \\ \cdot \\ E_{yi}(x_N) \\ 0 \end{bmatrix} \quad (2.40)$$

and

$$\bar{\bar{Z}}_{BMA} = \begin{bmatrix} A_{11} & B_{11} & A_{12} & B_{12} & \cdot & \cdot & A_{1N} & B_{1N} \\ C_{11} & D_{11} & C_{12} & D_{12} & \cdot & \cdot & C_{1N} & D_{1N} \\ A_{21} & B_{21} & A_{22} & B_{22} & \cdot & \cdot & C_{2N} & D_{2N} \\ \cdot & \cdot & \cdot & \cdot & \cdot & \cdot & \cdot & \cdot \\ C_{N1} & D_{N1} & C_{N2} & \cdot & \cdot & \cdot & C_{NN} & D_{NN} \end{bmatrix} \quad (2.41)$$

with the elements $(A_{mn}), (B_{mn}), (C_{mn})$ and (D_{mn}) given by (2.27)-(2.30). This new impedance matrix $\bar{\bar{Z}}_{BMA}$ is further decomposed into a strong matrix, $\bar{\bar{Z}}^s$, which contains the elements within a band centered around the diagonal, and a weak matrix $\bar{\bar{Z}}^w$ that contains the remaining elements. The half-bandwidth of this banded matrix is called b .

The k -th order solution, $\bar{X}^{(k)}$ of equation (2.23) is computed iteratively with

$$\bar{\bar{Z}}^s \bullet \bar{X}^{(1)} = \bar{V} \quad (2.42)$$

and

$$\bar{\bar{Z}}^s \bullet \bar{X}^{(k)} = \bar{V} - \bar{E}^{(k-1)} \quad (2.43)$$

until convergence is reached. The vector $\bar{E}^{(k)}$ in (2.42) is defined as $\bar{E}^{(k)} = \bar{\bar{Z}}^w \bullet \bar{X}^{(k)}$.

The error criteria is stated [54] by defining a "residual"

$$\bar{R}^{(n)} = \bar{V} - \bar{\bar{Z}}_{BMA} \bullet \bar{X}^{(n)} \quad (2.44)$$

Using equation (2.42)-(2.43), it is easy to show that $\bar{R}^{(1)} = -\bar{E}^{(1)}$, and $\bar{R}^{(n)} = \bar{E}^{(n-1)} - \bar{E}^{(n)}$. The truncation criterion of the iterative procedure is then defined to be [54]

$$\sqrt{\frac{\bar{R}^{(n)} \bullet \bar{R}^{(n)}}{\bar{V} \bullet \bar{V}}} \times 100 < e \quad (2.45)$$

This iterative method is much faster than the conventional matrix inversion in solving equations. Furthermore this BMIA method does not require to store the entire impedance matrix $\bar{\bar{Z}}_{BMA}$, which saves the computational memory requirements. In this method, only the strong matrix $\bar{\bar{Z}}^s$ is stored, and the elements of the weak matrix $\bar{\bar{Z}}^w$ are calculated for each iteration. This method allows then to solve the backscattering problem from very rough surfaces that involves large number of unknowns, and so large impedance matrix.

2.4. Scattered Field

When the fields on the surface are known, we can use the Huygen's principle to calculate the scattered field at an observation point \bar{r} [63]

$$E_s(\bar{r}) = \int_{S'} ds' [E_{y1} \hat{n}' \cdot \nabla_s G_1 - G_1 \hat{n}' \cdot \nabla_s E_{y1}] \quad (2.46)$$

The observation point defined by the vector \bar{r} , when far from the surface, can be defined by a distance r to the center of the profile and by a polar direction θ_s as shown in Figure 2.1. For any point on the surface defined by the vector \bar{r}' , we can then make the following approximation,

$$|\bar{r} - \bar{r}'| \approx r - x' \cos \theta_s - z' \sin \theta_s$$

By using the far field approximation for the two-dimensional Green's functions,

$$H_m^{(1)}(\xi) \approx \sqrt{\frac{2}{\pi\xi}} \exp\left[i\left(\xi - m\frac{\pi}{2} - \frac{\pi}{4}\right)\right], \text{ when } \xi \rightarrow +\infty \quad (2.47)$$

for $m = 0, 1$, with $\xi = k|\bar{r} - \bar{r}'| \approx kr - kx' \cos \theta_s - kz' \sin \theta_s$, we obtain the expression for the scattered field,

$$E_s(\bar{r}) = \frac{i\Delta x}{4} \sqrt{\frac{2}{\pi k}} \frac{\exp(ikr)}{\sqrt{r}} \exp\left(-i\frac{\pi}{4}\right) \times \sum_{m=1}^N \exp(-i\Phi_m) [ik_1 [f'(x_m) \sin \theta_s - \cos \theta_s] F_1(x_m) - F_2(x_m)] \quad (2.48)$$

with $\Phi_m = k_1(x_m \cos \theta_s + f(x_m) \sin \theta_s)$, and x_m defined in (2.15).

2.5. Backscattering Coefficient

The incoherent backscattering coefficient for a TE wave upon a one-dimensional rough surface is defined by analogy with the two-dimensional case as [2],

$$\sigma_{hh}^o = \frac{2\pi R(\langle |E_s|^2 \rangle - \langle E_s \rangle^2) \cos \theta_i / 2\eta_1}{P_{h,inc}} \quad (2.49)$$

where $\eta_1 = \sqrt{\frac{\mu_1}{\epsilon_1}}$ is the impedance of the medium above the profile, and $P_{h,inc}$ is the incident power. In equation (2.49), $\langle \rangle$ stands for an ensemble averaging performed over many realizations in the Monte-Carlo simulations.

The power of an incident TE tapered wave is defined as the average projection of the incident Poynting vector, \bar{S}_{inc} , along the normal of the profile, taken to be constant and equal to \hat{z} . We have then

$$P_{h,inc} = \int_{-\infty}^{+\infty} \langle \bar{S}_{inc} \rangle \cdot \hat{n} dx = \int_{-\infty}^{+\infty} \langle \bar{S}_{inc} \cdot \hat{z} \rangle \Big|_{z=0} dx \quad (2.50)$$

If $\bar{E}_{inc} = -\hat{y} \exp\left[i\bar{k} \cdot \bar{r}(1+w(\bar{r})) - (x+z \tan \theta_i)^2/g^2\right]$, along \hat{y} only, the averaged Poynting vector has its component along \hat{z} as

$$\langle \bar{S}_{inc} \cdot \hat{z} \rangle = \frac{1}{2i\omega\mu_1} \Re \left[E_{yi} \left(\frac{\partial E_{yi}}{\partial z} \right)^* \right] \quad (2.51)$$

where * denotes the complex conjugate, \Re and stands for the real part. Then, the power $P_{h,inc}$ is

$$P_{h,inc} = \frac{1}{2\eta_1} \sqrt{\frac{\pi}{2}} g \cos \theta \left[1 - \frac{0.5(1+2 \tan^2 \theta)}{k^2 g^2 \cos^2 \theta} \right] \quad (2.52)$$

Substituting (2.52) into (2.49), and averaging over M realizations to perform the ensemble averaging, we obtain the numerical expression of the one-dimensional backscattering coefficient for a tapered incident TE wave on a one-dimensional rough penetrable surface

$$\sigma_{hh}^o = \frac{2\pi R}{\sqrt{\frac{\pi}{2}} g \left[1 - \frac{0.5(1+2 \tan^2 \theta_i)}{k^2 g^2 \cos^2 \theta_i} \right]} \frac{1}{M} \left(\sum_{m=1}^M |E_s^{(m)}|^2 - \frac{1}{M} \left| \sum_{m=1}^M E_s^{(m)} \right|^2 \right) \quad (2.53)$$

where $E_s^{(m)}$ is the scattered field from the m-th realization.

Similarly, the backscattering coefficient for the one-dimensional rough penetrable surface in the TM case is given by

$$\sigma_{vv}^o = \frac{2\pi R (\langle |H_s|^2 \rangle - \langle H_s \rangle^2) \eta_1 \cos \theta_i / 2}{P_{v,inc}} \quad (2.54)$$

and the numerical expression based on Monte-Carlo simulations is

$$\sigma_{vv}^o = \frac{2\pi R}{\sqrt{\frac{\pi}{2}} g \left[1 - \frac{0.5(1 + 2 \tan^2 \theta_i)}{k^2 g^2 \cos^2 \theta_i} \right]} \frac{1}{M} \left(\sum_{m=1}^M |H_s^{(m)}|^2 - \frac{1}{M} \left| \sum_{m=1}^M H_s^{(m)} \right|^2 \right) \quad (2.55)$$

Chapter 3

Analytical Rough Surface Scattering Models

Three different analytical models of rough surface scattering, the Small Perturbation Method (SPM) [2], the Physical Optics (PO) approximation [3] and the Geometrical Optics (GO) approximation [2], will be used to validate the numerical scattering model described in Chapter 2. The profiles considered in the following sections are random rough surfaces that obey Gaussian distributed heights and slopes. These one-scale profiles are statistically characterized by the correlation length l , the root-means-square (rms) height σ , and the correlation function in the horizontal dimension $C(x')$.

3.1. Small Perturbation Method

The Small Perturbation Method [2] is based on perturbation approach to compute analytically the backscattering cross-section of an incident wave on a slightly rough surface. This perturbation theory expands field solutions in perturbation series assuming that $k_{1iz}f(x')$, $k_{2z}f(x')$, and $\frac{\partial f(x')}{\partial x'}$ are small parameters. k_{1iz} is the \hat{z} component of the incident wave vector in medium 1, and k_{2z} the \hat{z} component of the transmitted wave vector in medium 2 (Figure 2.1). Thus, the SPM model requires the surface heights be much smaller than a wavelength and small surface slopes for rough surfaces with smoother profiles. The zeroth order solution consists of the specularly reflected waves, and the first

order term contributes only to the incoherently scattered fields. In the following section will be presented only the first order SPM results for backscattering coefficients, which were proved to be valid through comparison with numerical methods for surfaces with Gaussian correlation function [50].

Ulaby *et al* [3] gave the analytical expressions for the SPM range of validity in terms of the rms height σ and the slope as

$$\begin{aligned} k_1 \sigma &< 0.3 \\ rms\ slope &< 0.3 \end{aligned} \quad (3.1)$$

Following [2], a backscattering cross-section for the one-dimensional case of rough surface scattering is defined as the ratio of the scattered power of polarization q in the direction \bar{k}_s , to the intercepted incident power of polarization p by the profile in the direction $-\bar{k}_s$, and averaged over 2π . For the geometry of Figure 2.1, and HH polarization, the backscattering coefficient is given as,

$$\sigma_{hh}^o = 8\pi k_1^3 \cos^4 \theta_s |R_{hh}|^2 W(2k_1 \sin \theta_i) \quad (3.2)$$

with $W(q)$ being the Fourier transform of the autocorrelation function $C(x')$ of the profile

$$W(q) = \frac{\sigma^2}{2\pi} \int_{-\infty}^{+\infty} C(x') \exp(-iqx') dx' \quad (3.3)$$

$|R_{hh}|$ is the Fresnel reflection coefficient for the TE wave, as expressed in equation (3.10).

For the VV polarization, we have

$$\sigma_{vv}^o = 8\pi k_1^7 \cos^4 \theta_s |A|^2 W(2k_1 \sin \theta_i) \quad (3.4)$$

where

$$A = \frac{(k_2^2 - k_1^2)(k_2^2 \sin \theta_i + k_2^2 - k_1^2 \sin^2 \theta_i)}{(k_2^2 k_1 \cos \theta_i + k_1^2 \sqrt{k_2^2 - k_1^2 \sin^2 \theta_i})^2} \quad (3.5)$$

3.2. Physical Optics Approximation

In the Kirchhoff approximation, the rough surface is described as a succession of infinite planes, which scatter energy in the specular direction. The tangential surface field on the surface profile is assumed to be that would exist on a plane tangent to each point on the surface [2]. Thus, given the incident wave, the height and the first derivatives of the profiles, we can determine in each point the TE and TM components of the reflected field. The total tangential field on the surface, sum of the incident and reflected waves, is then known, and constitutes the solution of the integral equations (1.6)-(1.9). This theory is applicable to surfaces with gentle undulations whose "average horizontal dimension is large compared with the incident wavelength" [3]. When considering one-scale surface profiles, their correlation length must be larger than the wavelength, and with a large radius of curvature relative to the incident wavelength at every point on the surface. Another approximation is made in the Physical Optics that leads to a simpler analytical solution. This approximation applies to profiles with small slopes and a rms height, such that $2k_1 \cos \theta_i$ is moderate or small [57]

The validity range for this model has been given by Ulaby *et al* [3] and is stated as follows for a Gaussian correlation function,

$$\begin{aligned} k_1 l &> 6 \\ l^2 &> 2.76 \sigma \lambda_1 \\ rms \text{ slope} &< 0.25 \end{aligned} \quad (3.6)$$

For a random rough surface with a correlation function $C(x')$, under the Physical Optics approximation, the co-polarized backscattering coefficient for polarization pp is composed of two terms, $\sigma_{inc,pp}^o$ and $\sigma_{slope,pp}^o$, as [3]

$$\sigma_{pp}^o = \sigma_{inc,pp}^o + \sigma_{slope,pp}^o \quad (3.7)$$

where

$$\sigma_{inc,pp}^o = 2k_1 |R_{pp}|^2 \cos^2 \theta_i \exp(-K_o) \sum_{n=1}^{\infty} \frac{(K_o)^n}{n!} \left(\int_0^{+\infty} C^n(u) \cos(q_x u) du \right) \quad (3.8)$$

and

$$\begin{aligned} \sigma_{slope,pp}^o = i 2k_1 q_z \sigma^2 & \left[|R_{pp}|^2 \sin \theta_i \cos \theta_i + \Re(R_{pp} R_{pp1}^*) \cos^2 \theta_i \right] \\ & \times \exp(-K_o) \sum_{n=0}^{\infty} \frac{(K_o)^n}{n!} \left(\int_0^{+\infty} \frac{dC}{du} C^n(u) \cos(q_x u) du \right) \end{aligned} \quad (3.9)$$

In the above expressions,

$$R_{hh} = \frac{\eta_2 \cos \theta_i - \eta_1 \cos \theta_t}{\eta_2 \cos \theta_i + \eta_1 \cos \theta_t} \quad (3.10)$$

$$R_{vv} = \frac{\eta_1 \cos \theta_i - \eta_2 \cos \theta_t}{\eta_2 \cos \theta_i + \eta_1 \cos \theta_t} \quad (3.11)$$

$$R_{hh1} = -R_{hh} \frac{\eta_2 \sin \theta_i + \eta_1 \sin \theta_t}{\eta_2 \cos \theta_i + \eta_1 \cos \theta_t} \quad (3.12)$$

$$R_{vv1} = -\frac{[\eta_1 \sin \theta_i - \eta_2 \sin \theta_t - R_{vv}(\eta_1 \sin \theta_i + \eta_2 \sin \theta_t)]}{\eta_1 \cos \theta_i + \eta_2 \cos \theta_t} \quad (3.13)$$

with θ_i the transmitted angle, and $\eta_j = \sqrt{\mu_j / \epsilon_j}$ the impedance of medium j, for j=1 or 2, $q_x = -2k_1 \sin \theta_i$, $q_z = -2k_1 \cos \theta_i$, $K_o = 4k_1^2 \cos^2 \theta_i \sigma^2$, and * stands for the complex conjugate.

In Appendix, the Physical Optics model will be implemented for both Gaussian and exponential profiles.

3.3. Geometrical Optics Approximation

The Geometrical Optics approximation is another analytical rough surface scattering theory derived from the Kirchhoff approximation [2]. Two further approximations are made, the "stationary-phase approximation" and the "deep phase modulation" [57]. The use of the "stationary-phase approximation" means that the scattering can occur only along directions for which there are specular points on the surface. Hence, local diffraction effects are excluded. The "deep phase modulation" assumption means that only profiles with large rms height are considered, such that $2k_1 \cos \theta_i$ is large. This model does not include multiple scattering and shadowing, and yields a surface scattering that is purely noncoherent, and a cross-polarized backscattering coefficient equals to zero. When the rms height decreases, some scattered energy begins to appear in the coherent component, and the PO approximations must be made.

The conditions of validity of this theory are given by Ulaby *et al* [3]

$$\begin{aligned}
 k_1 l &> 6 \\
 l^2 &> 2.76 \sigma \lambda_1 \\
 (2k_1 \cos \theta_i \sigma)^2 &> 10 \\
 (2k_2 \cos \theta_i \sigma)^2 &> 10
 \end{aligned} \tag{3.14}$$

The backscattering coefficients for one-dimensional rough penetrable surface, under the Geometrical Optics approximations is given as, [57]

$$\sigma_{hh}^o = \sigma_{vv}^o = \sqrt{\frac{\pi}{2}} |R_{pp}(0)|^2 \frac{1}{m \cos^3 \theta_i} \exp\left(-\frac{\tan^2 \theta_i}{2m^2}\right) \quad (3.15)$$

where $R_{pp}(0)$ is the Fresnel reflection coefficient evaluated at normal incidence, and $m = \sigma\sqrt{|C''(0)|}$ is the rms slope of the given profile.

We can see that the expression does not apply to rough surfaces for which the second derivative of the correlation function, $C(x')$, at the origin is not defined. Hence, only the case of a Gaussian profile will be studied, whose rms slope is simply given as

$$m = \sigma\sqrt{|C''(0)|} = \frac{\sqrt{2}\sigma}{l} \quad (3.16)$$

which can be substituted in equation (3.15) to obtain the backscattering coefficients.

Chapter 4

Numerical Simulation and Comparison

Several numerical works have been done in the past with perfectly conducting surfaces [21]. These numerical calculations for perfectly conducting profiles need only half as many unknowns as for the penetrable case, since the tangential electric field on the surface must be set equal to zero to match the boundary conditions. But this impenetrable case that results in a limited CPU times, does not apply to the study of soil moisture where the ground surface is characterized by the finite permittivity of the soil.

In the study of penetrable case [64], profiles with Gaussian auto-correlation function were considered to limit the CPU time in calculation too. Indeed, in Ogilvy [65], the Gaussian profile is shown to be less rough than the exponential profile with the same correlation length and rms height. The CPU time and the available computer memory appear to be the factors that limit the use of the Method of Moments as a tool to study the backscattering for penetrable rough surface case. The information about the parameters leading for a given profile to a minimum CPU time or memory storage, would be hence helpful to the study of rough surface scattering.

The following work will provide an idea of the parameters needed to use efficiently the MOM in the remote sensing of soil moisture problem. Both Gaussian and exponential profiles with different roughness will be investigated in the penetrable case. In each of the

three domains of validity for the SPM, PO and GO analytic models, the HH and VV backscattering coefficient will be computed both by the Method of Moments and the analytical expressions, and comparisons will be performed to validate the numerical model. In each case, the issues considered are the effect of the window parameter g , of the finite length of the profile on the convergence of backscattering results. The necessary number of realizations and the influence of the bandwidth, b , in the BMIA method are investigated too.

4.1. Profile Generators

The profiles are generated by a code using a Moving Average Process described by Ogilvy [66]. This method allows to generate one-scale profiles statistically defined by: the correlation length l , the rms height σ , and the correlation function $C(x)$ (Gaussian, or exponential). Furthermore, they obey Gaussian distributed heights and slopes. A brief description of this method is given below.

A given rough profile is represented by a set of $2N+1$ correlated points, $(z_i)_{i=-N,N}$, giving the height of the profile relative to the flat plane at $z = 0$. This correlated set of points is obtained from an initial set of uncorrelated random number $(r_i)_{i=-N,N}$, with a Gaussian distribution of zero mean. The desired rms height σ is defined by

$$\sigma = \frac{1}{2N+1} \sum_i r_i^2 \quad (4.1)$$

where $(r_i)_{i=-N,N}$ are correlated by applying a sliding discretized weighting function $(w_i)_{i=-M,M}$ of length $2M+1$ ($M \ll N$), such as

$$z_i = \sum_{j=-M}^M w_j r_{i+j} \quad (4.2)$$

These weights $(w_i)_{i=-M,M}$ depend on the given correlation function $C(x)$. The Fourier transform of the correlation function, or power spectrum $W(k)$, is first computed according to

$$W(k) = \frac{1}{2\pi} \int_{-\infty}^{+\infty} C(x) \exp(ikx) dx \quad (4.3)$$

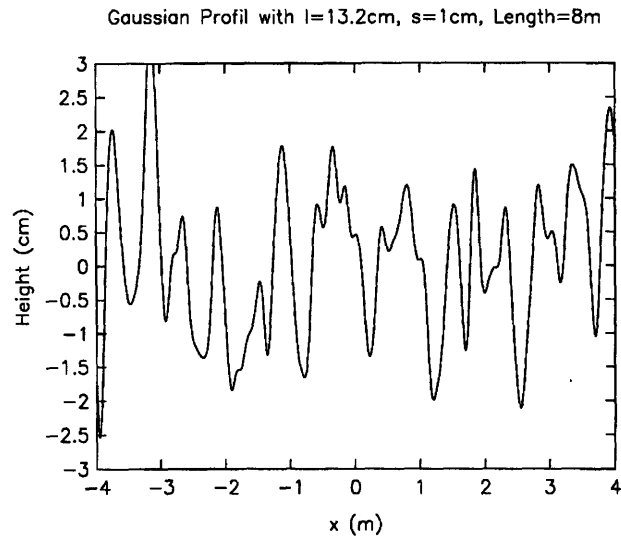
Then, the moving average weight are determined by computing the inverse Fourier transform of the square-root of $W(k)$. The following table gives this process for both the Gaussian and exponential case.

Correlation Function $C(x)$	Power Spectrum $W(k)$	(w_j) Fourier Transform of $\sqrt{W(k)}$
$\exp\left(-\frac{x^2}{l^2}\right)$	$\frac{1}{2\sqrt{\pi}} \exp\left(-k^2 l^2 / 4\right)$	$\propto \exp\left(\frac{-2(i\Delta x)^2}{l^2}\right)$
$\exp\left(-\frac{ x }{l}\right)$	$\frac{1}{\pi} \frac{l}{1+k^2 l^2}$	$\propto K_o\left(\frac{ i\Delta x }{l}\right)$

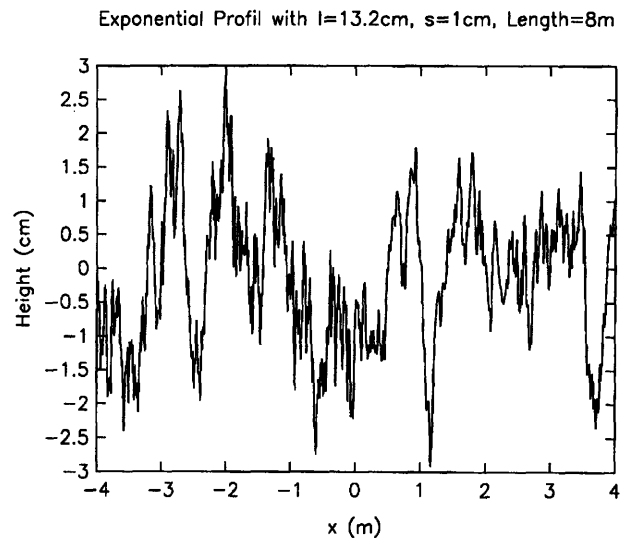
Table 4.1.1. Moving Average in Gaussian and exponential case.

where K_o is the modified Bessel function of the zeroth order.

According to Ogilvy [64], the sampling interval Δx of a profile must be less than one tenth of the considered correlation length to record the short-range difference between Gaussian and exponential profiles. This requirement will be met in all our simulations. In Figure 4.1 two samples of a Gaussian and an exponential profile are plotted. We observe that the fluctuations of the two profiles, even with identical correlation length and rms height, are quite different. The exponential surface has been characterized by "short-range, small amplitude fluctuations" [64], whereas the Gaussian profile appears to be smoother on this scale length. In Figure 4.2 and 4.3, the correlation functions deduced from sets



(a)



(b)

Figure 4.1. (a) Gaussian, (b) Exponential Profile.

of computer generated profiles, shown as dotted curves, are compared with their theoretical forms shown as solid curves, for both Gaussian and exponential cases. In Figure 4.2, the profile is for a Gaussian correlation function; a profile length of 80λ , correlation length $l=13.2$ cm, and rms height $\sigma=1$ cm are used for the simulation. The number of sampling points per profile is 800 corresponding to an equal sampling length of $\Delta x=l/13$. In Figure 4.3, the profiles are defined by the same parameters as Figure 4.2, but with an exponential correlation function. We observe that the exponential function falls off faster, implying a loss of correlation more rapid. On the other hand, the Gaussian curve falls off slower, leading to a longer scale of correlation. The exponential surfaces appear thus to have roughness on a finer scale than Gaussian profiles, even with identical rms height, and correlation length.

From a numerical point of view, in both Gaussian and exponential cases, the synthesized correlation function is computed by averaging over 80 realizations. We note that the numerical results agree very well with the theoretical results, both for Gaussian and exponential profile. The small discrepancy is due to the finite length of the profile used that leads to a spectral leakage. The statistical properties of these profiles can be improved by generating either longer profiles, or more realizations at a given length.

This small discrepancy between the nominal statistical parameters and the estimated statistical parameters from the set of generated realizations must be taken into account when the analytical models for rough surface scattering are used. Hence, in the following comparison process, the statistical parameters chosen as input for analytical models are not the theoretical one, but those computed numerically from the generated profiles.

We define the estimated rms height $\hat{\sigma}$ as

$$\hat{\sigma}^2 = \frac{1}{L} \left\langle \int_{-L/2}^{L/2} f^2(x) dx \right\rangle \quad (4.4)$$

Gaussian Autocorrelation Function

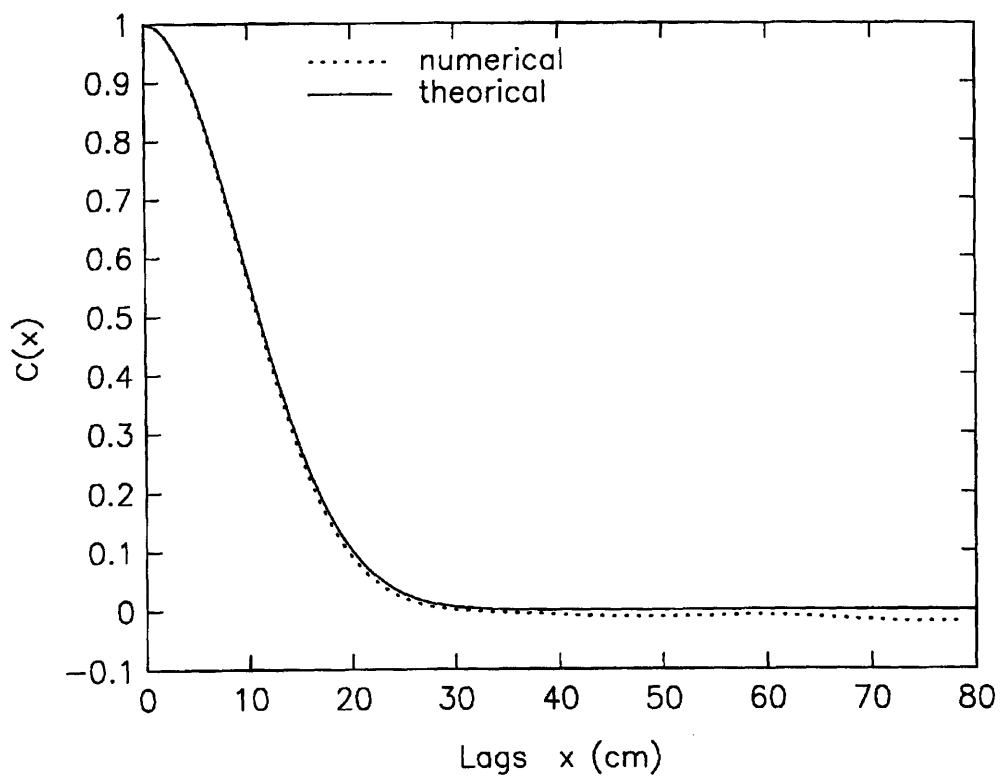


Figure 4.2. Correlation function of a generated Gaussian profile compared to the theoretical correlation function.

Exponential Autocorrelation Function

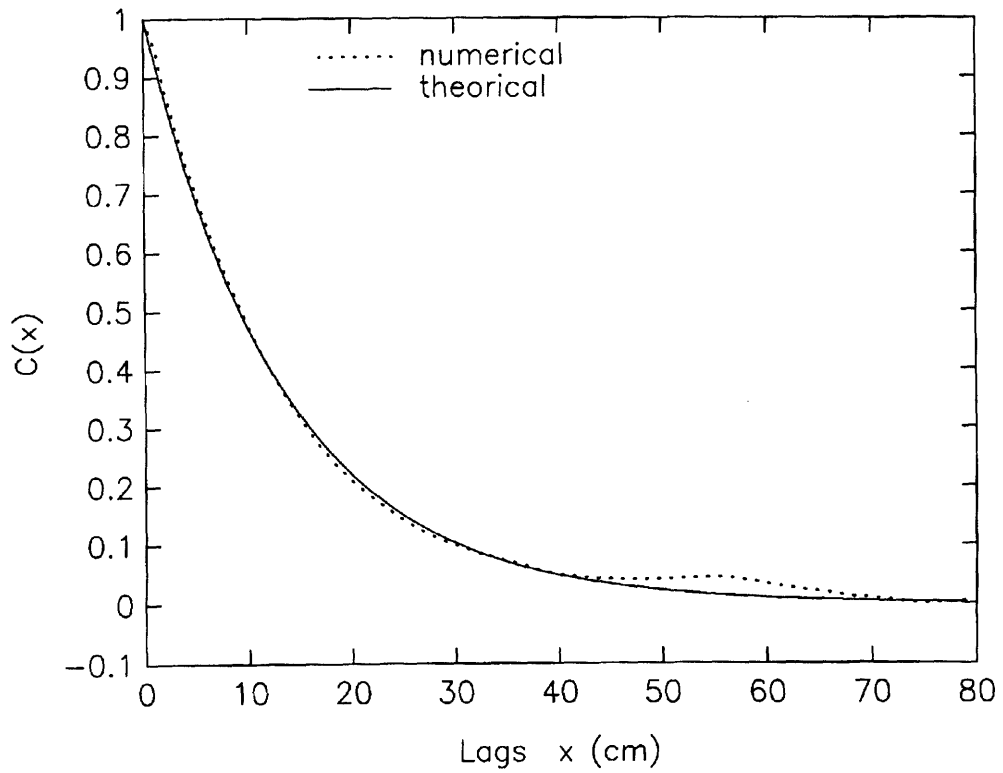


Figure 4.3. Correlation function of a generated exponential profile compared to the theoretical correlation function.

and the estimated rms slope \hat{m} as

$$\hat{m}^2 = \frac{1}{L} \left\langle \int_{-l/2}^{l/2} \left(\frac{df}{dx} \right)^2 dx \right\rangle \quad (4.5)$$

where the angular brackets denotes ensemble average. In the case of Gaussian correlation function, the rms slope is related to the correlation length by

$$m = \sigma \sqrt{|C''(0)|} = \frac{\sqrt{2}\sigma}{l} \quad (4.6)$$

By substituting (4.4) and (4.5) in (4.6), we obtain an estimate of \hat{l} for Gaussian profile. For the exponential profile, the correlation function will be computed numerically from the ensemble of realizations, and the estimated of the correlation length will be derived graphically. The ensemble averaging in (4.4) and (4.5) is performed over many realizations.

4.2. Simulations and Results

These simulations were performed on a DEC 3000-M 400 workstation with 416 Megabytes of RAM and an ability to perform approximately 375 MFLOPs per second.

4.2.1. Small Perturbation Method

The first set of profile considered has its statistical property within the approximate domain of validity of the Small Perturbation Method as stated in Section 3.1. The statistical parameters of the studied surface are listed in the Table 4.2.1.

Frequency	$5/3 \text{ GHz}$
Correlation function	exponential/Gaussian
l	4 cm
σ	1 mm
ϵ_2	$(3,0.1) \text{ or } (9,1.0)$

Table 4.2.1. Frequency and statistical parameters of the profile.

For a given set of parameters, (length of the profile, number of unknowns, BMIA bandwidth, windowing parameter) the number of realizations used increases until the convergence is reached. Figure 4.4 shows the variations of the HH backscattering coefficients, for different incident angles, as a function of the number of realizations. These results are for a profile length of 80λ , up to 160 realizations, and a level of discretization of 10 unknowns per wavelength. We can observe easily the convergence of our results when the number of realizations increases. Therefore, when there is convergence, a minimum number of realizations required can be defined. This same study has been made for the profile length of 20λ and 40λ , both for exponential and Gaussian correlation functions.

The bandwidth used in the BMIA approach is increased from 80 to 170 points without noticing any variations of the backscattering coefficients. This parameter sets the number of points that influence the current sources around a given point M. The minimum bandwidth b necessary to reach convergence should logically depend on the correlation length of the profile. We will see in the next two sections that this assumption is verified. In this case where $l = 4 \text{ cm}$, a bandwidth of $20l$ or 80 points was found to be sufficient.

The profile length is increased from 10λ to 100λ . In Figure 4.5, a comparison is illustrated between the numerical results for three different lengths of profile $L=20\lambda$, $L=40\lambda$ and $L=80\lambda$, with respective 200 and 160 realizations, for the exponential case.

Study of convergence $f=5/3\text{GHz}$ $kl=1.396$ $ks=0.035$ $\text{eps}=(3,0.1)$

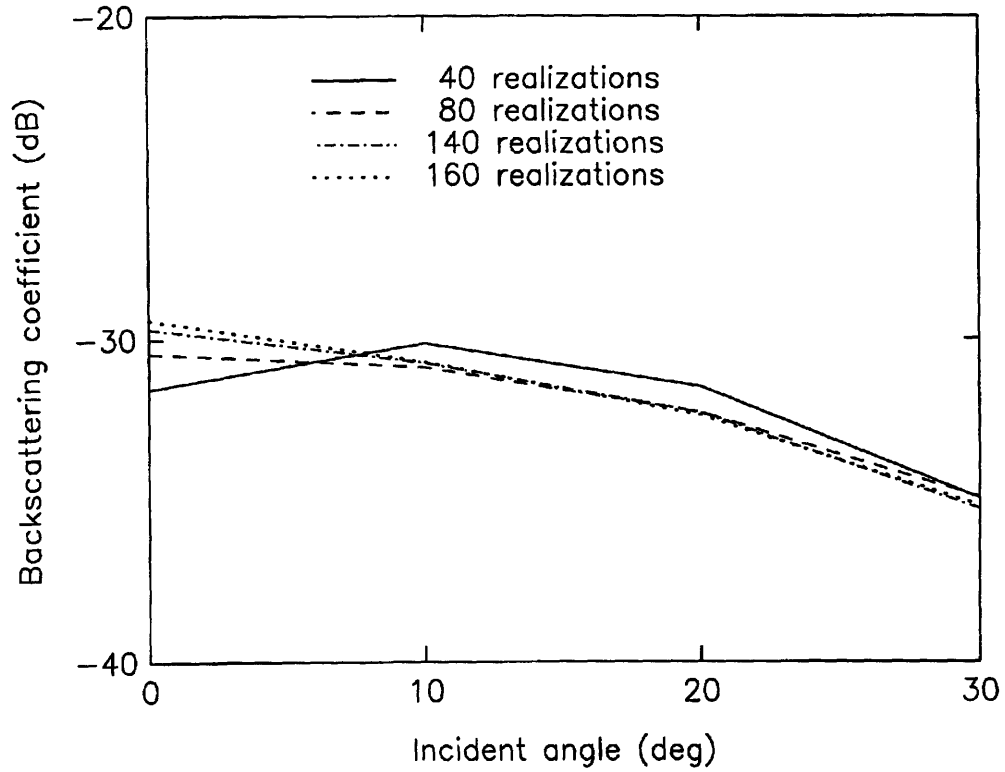


Figure 4.4. TE case: Study of convergence as a function of the number of realizations for an exponential profile with $L=80\lambda$, $kl=1.396$, $k\sigma=0.035$, and $\epsilon_2=(3,0.1)$.

Study of convergence $f=5/3\text{GHz}$ $kl=1.396$ $k\sigma=0.035$ $\epsilon_s=(3,0.1)$

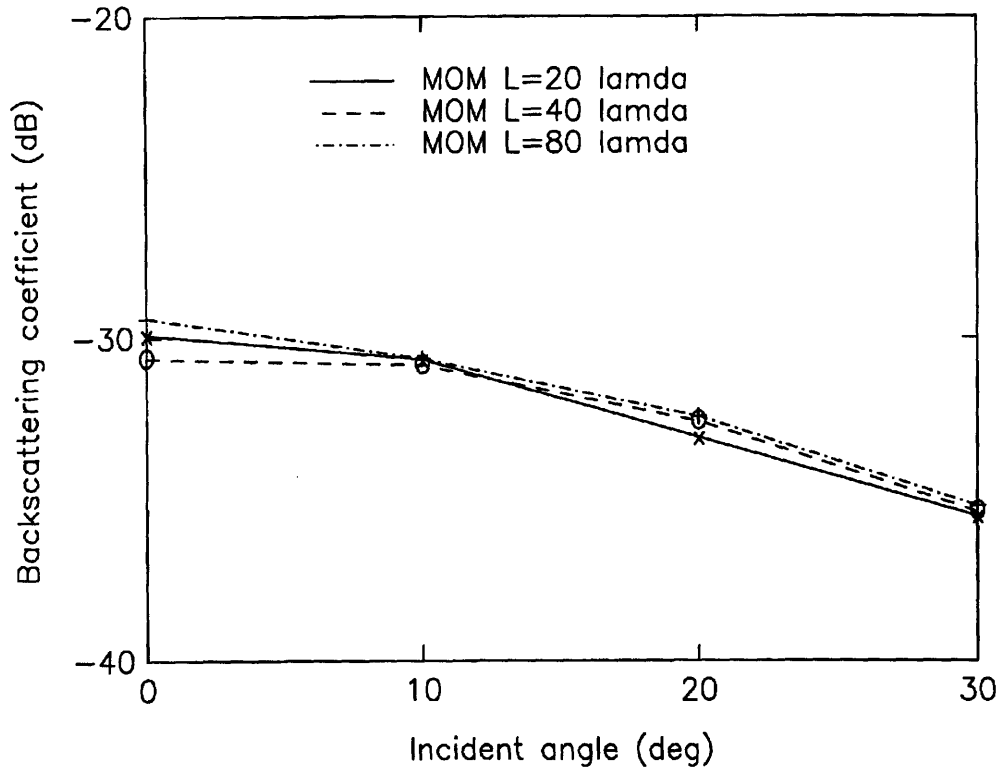


Figure 4.5. TE case: Study of convergence as a function of the length of surface for an exponential profile with $kl=1.396$, $k\sigma=0.035$, and $\epsilon_2=(3,0.1)$.

We can observe that there is no significant difference greater than 0.4 dB on the whole range of incident angle. Our estimation is then stable when we increase the length of the profile. The comparison with the analytical model is then made with the shortest profile of 20λ . However, between 20λ and 40λ , the results of 40λ profile shows better estimation only for the zero degree incidence angle. But this slight improvement corresponds to a four-times increase in CPU time used. It may therefore not be judged necessary to use so long profile depending on the applications considered. For a profile length of 20λ , 200 realizations are sufficient to reach a 0.2 dB difference from the analytical values, except for the normal incident angle. Indeed, in this case, we have a difference of 0.5 dB between them. However, in practical applications, the normal incidence case is never studied, since the non-coherent backscattering is difficult to separate from the specular reflection.

The study of convergence leads then to the following choice of parameters for the MOM solution of exponential rough surfaces in the SPM range

length of the profile	number of unknowns	window parameter g	BMIA bandwidth b
$20 \lambda / 90 l$	20 per λ	$\frac{L}{4}$	80 pt. or $20l$

Table 4.2.2. Parameters used for the numerical simulations for Gaussian case.

The one-dimensional analytical SPM results are calculated using the following estimated values of the correlation length, graphically determined, and rms height computed by (4.4).

$\hat{\sigma}$	1.055 mm
\hat{l}	4.1 cm

Table 4.2.3. Estimated surface statistical parameters.

Figure 4.6 compares the MOM results calculated using the parameters in Table 4.2.2 to those values obtained using the analytical SPM model, for the exponential profile case. These values are given in the Table 4.2.4. We note that the numerical results and the SPM results match very well, since they are within 0.2 dB difference for all angles considered, except for the normal incidence.

Incident Angle	Numerical results	Analytical results
0	-29.90	-29.4
10	-30.67	-30.52
20	-33.09	-32.95
30	-35.54	-35.52

Table 4.2.4. TE backscattering coefficients of the MOM and the analytical SPM method for the exponential correlation function case.

The study of the Gaussian case leads to the same numerical parameters as stated in Table 4.2.2. The only difference concerns the minimum number of realizations required to reach convergence. Figure 4.7 shows the convergence of the numerical backscattering coefficient with the number of realizations for a Gaussian profile of $L=20\lambda$. We note that a smaller number of realizations is needed for this Gaussian profile to reach the desired level of convergence. Indeed, after 140 realizations, compared to 200 realizations for the exponential case, the difference between MOM results and SPM results is less than 0.2 dB. In this case, the one-dimensional analytical SPM model is used with the following estimated values of the correlation length and rms height, computed from (4.2) and (4.6).

Validation $f=5/3\text{GHz}$ $kl=1.396$ $k\sigma=0.035$ $\epsilon_2=(3,.1)$ expo

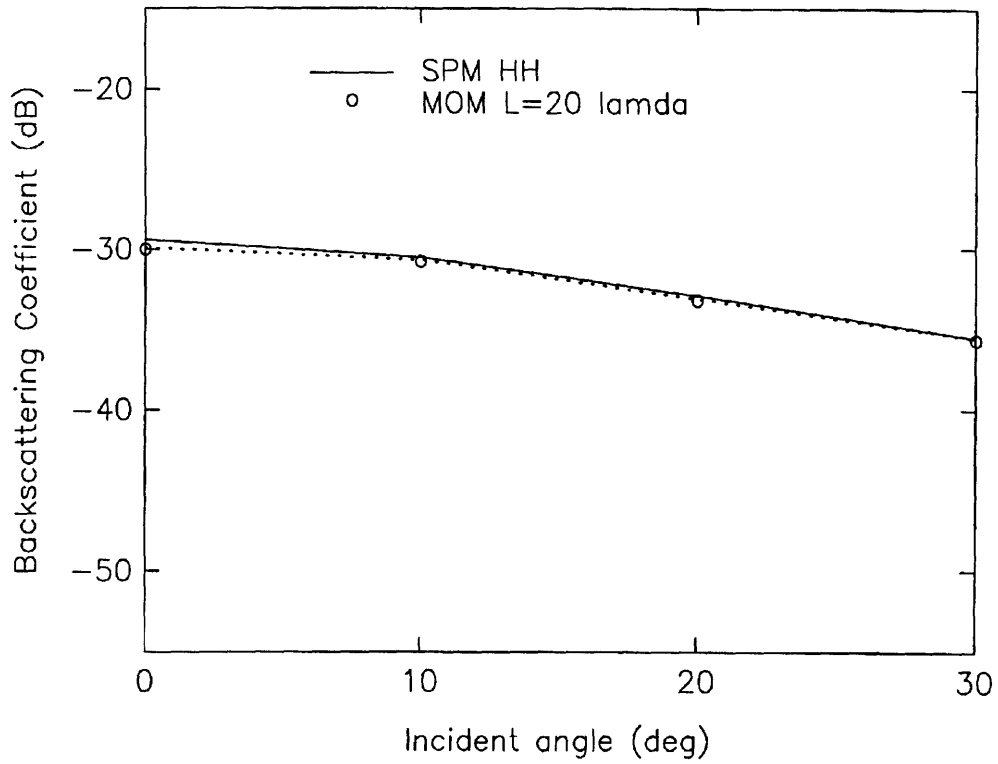


Figure 4.6. TE case: Comparison between MOM results and Small Perturbation Method model for an exponential profile of $kl=1.396$, $k\sigma=0.035$, and $\epsilon_2=(3,0.1)$.

Study of convergence $f=5/3\text{GHz}$ $kl=1.396$ $k\sigma=0.035$ $\epsilon_2=(3,0.1)$

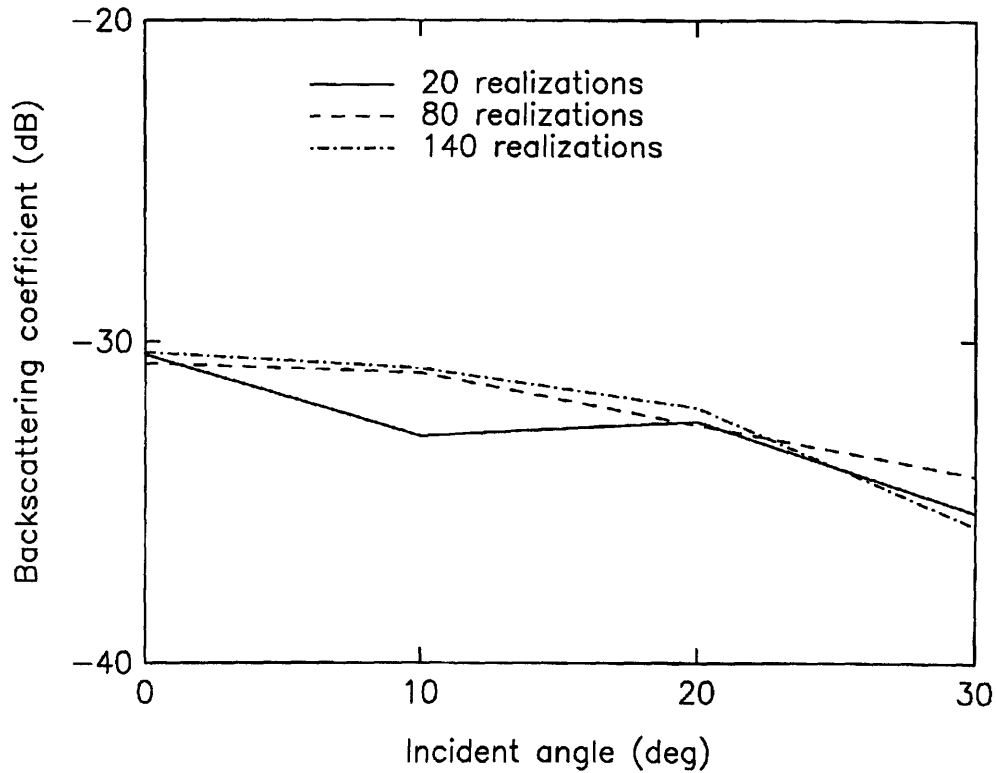


Figure 4.7. TE case: Study of convergence in function of the number of realizations for a Gaussian profile with $L=20\lambda$, $kl=1.396$, $k\sigma=0.035$, and $\epsilon_2=(3,0.1)$.

$\hat{\sigma}$	<i>1mm</i>
\hat{l}	<i>4cm</i>

Table 4.2.5. Estimated surface statistical parameters.

Figure 4.8 compares the MOM results obtained with the parameters given in Table 4.2.2 to the values obtained with the analytical SPM model for the Gaussian profile case. These values are summarized in the Table 4.2.6. As for the exponential case, the MOM results and the SPM results match well, their difference being within 0.3 dB for all angles considered.

Incident Angle	Numerical results	Analytical results
0	-30.61	-30.32
10	-30.98	-30.82
20	-32.07	-32.07
30	-33.85	-33.69

Table 4.2.6. TE backscattering coefficient of the MOM and of the analytical SPM method for the Gaussian correlation function case.

For "smooth surfaces", with short correlation length and small rms height, the influence of the auto correlation function on the choice of numerical parameters does not appear clearly. A greater number of realizations needed to reach convergence is the only difference between the exponential and Gaussian profiles. However, it seems to be logical since these profiles differ only in the short-range. Indeed, the wavelength acts like a yardstick on the profile, and is unable to see finer details than its own length. In our case, the correlation length, equal to 0.22λ , is not long enough for the wavelength to see such a difference in the short-range scale.

Validation $f=5/3\text{GHz}$ $kl=1.396$ $k\sigma=0.035$ $\epsilon_2=(3,.1)$ gauss.

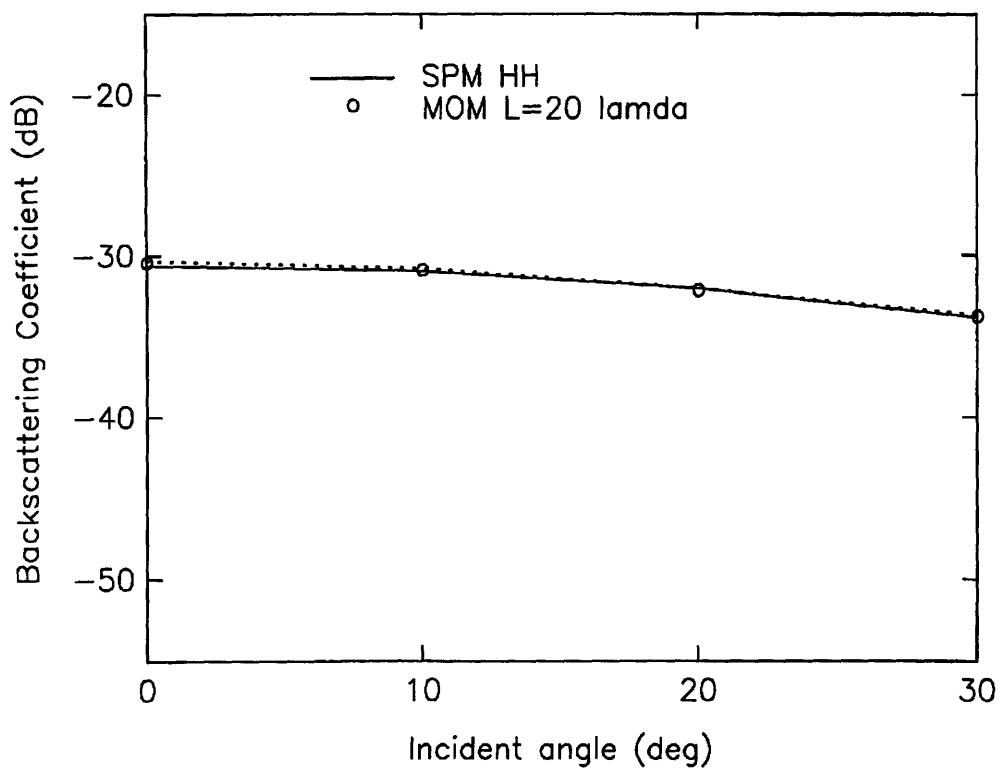


Figure 4.8. TE case: Comparison between MOM results and Small Perturbation Method model for a Gaussian profile of $kl=1.396$, $k\sigma=0.035$, and $\epsilon_2=(3,0.1)$.

Similar sensitivity studies are performed for the one-dimensional TM case and give similar results. In Figures 4.9 and 4.10 analytical SPM results and numerical MOM results are compared for a length of 20λ , with Gaussian and exponential profiles respectively. The characteristics of the profiles are given in Table 4.2.1. The MOM results match the analytical SPM values, with a difference less than 0.3 dB, for angles between the normal incidence and 40 degrees. It seems that the polarization, for smoother surfaces, does not affect the choice of the numerical parameters.

The effect of the dielectric constant on the choice of the numerical parameters is also assessed by considering different values of ϵ_2 . We have found that the same choice of parameters leads to similar level of convergence compared to SPM. In Figures 4.11 and 4.12, can be observed the comparison between MOM results and SPM estimations, for $\epsilon_2=(9,1)$, for HH polarization, respectively for Gaussian and exponential case. In the next section, we examine another type of profile, with a longer correlation length in term of wavelength, taken into the domain of validity of the Physical Optics Approximation.

4.2.2. Physical Optics Approximation

The second set of profiles considered has its statistical property in the Physical Optics domain of validity as described in Section 3.2. The rough surface statistical properties that will be considered are given in the Table 4.2.8.

Frequency	<i>3GHz</i>
Correlation function	exponential/Gaussian
<i>l</i>	<i>13.2cm</i>
<i>σ</i>	<i>1cm</i>
ϵ_2	(3,0.1) or (9,1.0)

Table 4.2.7. Frequency and statistical parameters of the profile.

Validation $f=5/3\text{GHz}$ $kl=1.396$ $k\sigma=0.035$ $\epsilon_s=(3,.1)$ gaus.

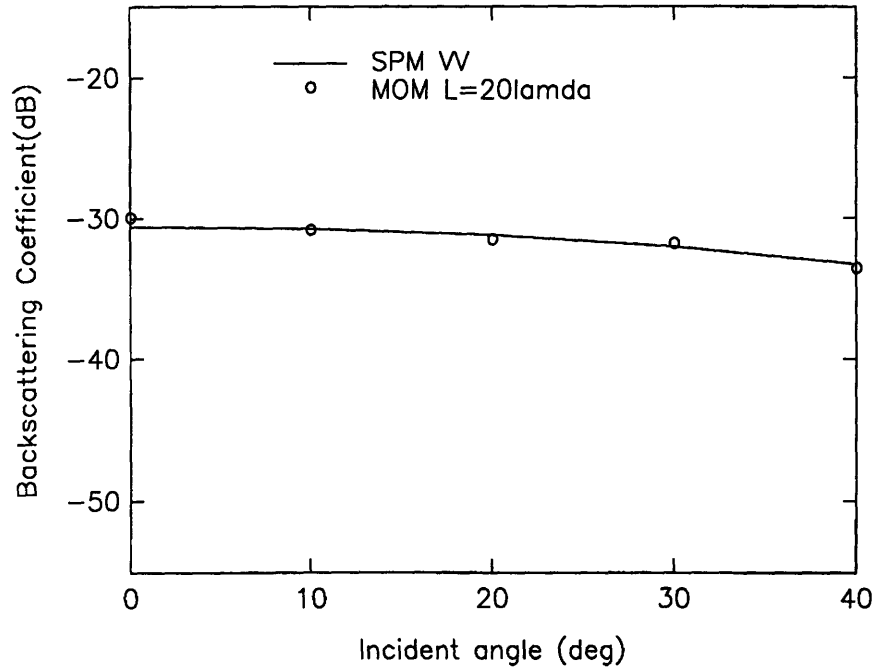


Figure 4.9. TM case: Comparison between MOM results and Small Perturbation Method model for a Gaussian profile of $kl=1.396$, $k\sigma=0.035$, and $\epsilon_2=(3,0.1)$.

Validation $f=5/3\text{GHz}$ $kl=1.396$ $k\sigma=0.035$ $\epsilon_s=(3,.1)$ expo.

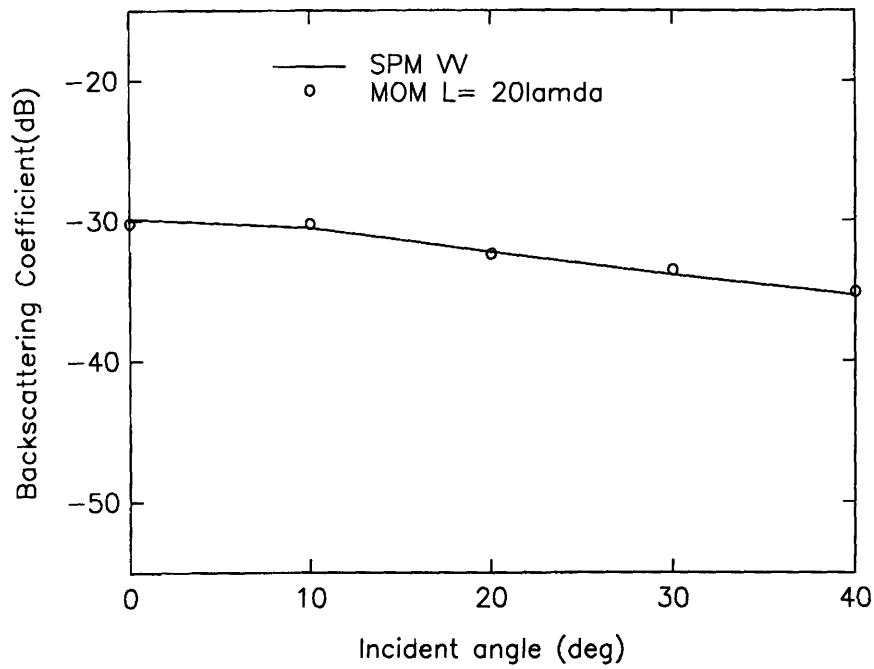


Figure 4.10. TM case: Comparison between MOM results and Small Perturbation Method model for an exponential profile of $kl=1.396$, $k\sigma=0.035$, and $\epsilon_2=(3,0.1)$.

Validation $f=5/3\text{GHz}$ $kl=1.396$ $k\sigma=0.035$ $\epsilon_2=(9,1)$ gaus.

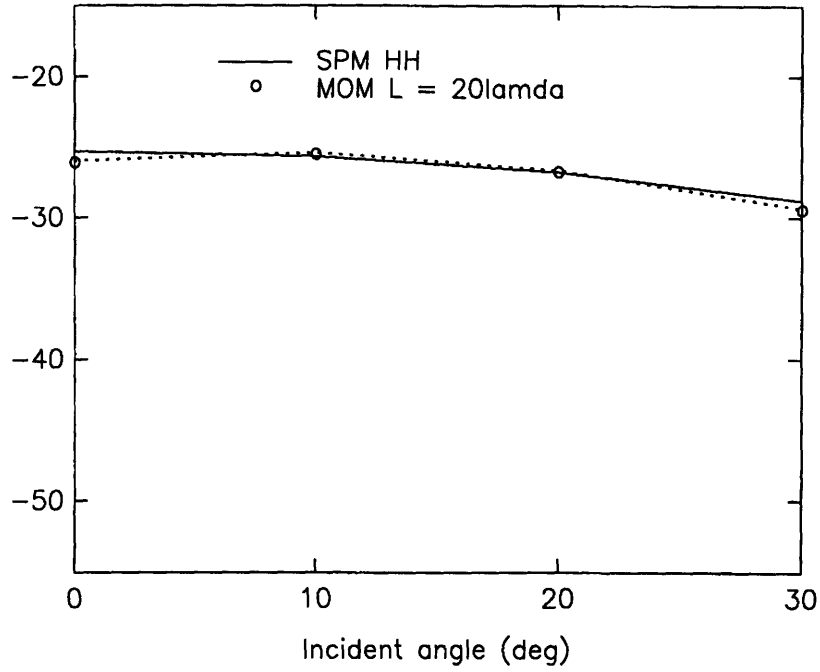


Figure 4.11. TE case: Comparison between MOM results and Small Perturbation Method model for a Gaussian profile of $kl=1.396$, $k\sigma=0.035$, and $\epsilon_2=(9,1)$.

Validation $f=5/3\text{GHz}$ $kl=1.396$ $k\sigma=0.035$ $\text{eps}=(9,1)$ exp.

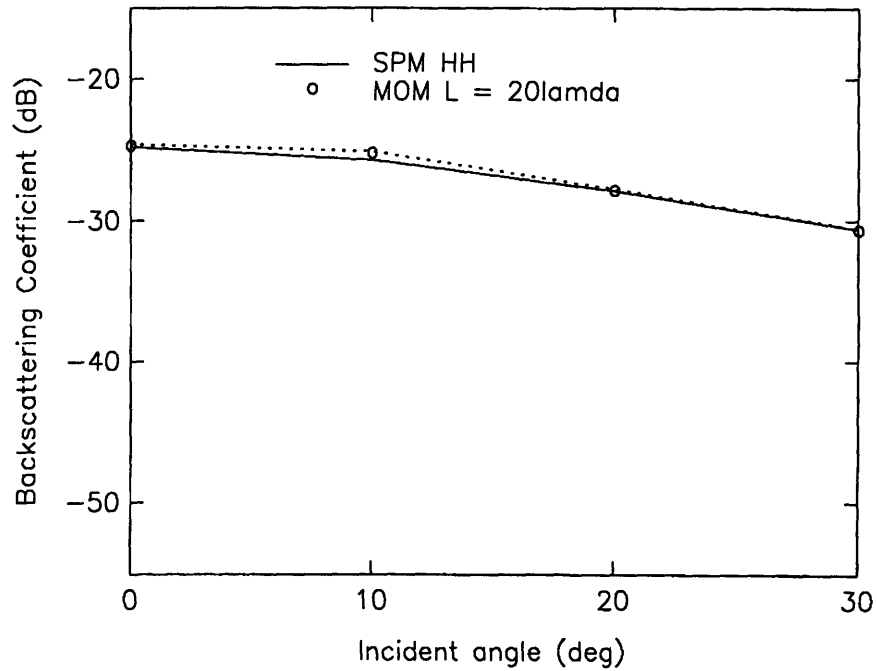


Figure 4.12. TE case: Comparison between MOM results and Small Perturbation Method model for an exponential profile of $kl=1.396$, $k\sigma=0.035$, and $\epsilon_2=(9,1)$.

Profiles with an exponential correlation function will be examined first.

The profile length is increased from 20λ to 100λ , to determine the minimum length required for the MOM. In Figure 4.13, the convergence of the HH backscattering coefficient, σ_{hh}^o , is shown as a function of the number of realizations, for three different profile lengths 40λ , 80λ , and 100λ up to 100 realizations, and the angle of incidence at 20 degrees. These convergence studies are also made for other incidence angles. However, a profile of length 20λ , or 15 correlation length, leads to divergent results. This study shows us that the profile chosen must be long enough compared to the correlation length in order convergence to be reached. A length of profile of 80λ appears to be satisfactory, since after 160 realizations, we have less than 0.2 dB in difference for all the angles considered except at normal incidence. In Figure 4.14. the MOM results for $L=40\lambda$ and $L=80\lambda$ are compared with the analytical PO for the HH backscattering coefficients. It shows that the length 40λ is not long enough to capture the statistic of these exponential profiles.

The BMIA bandwidth is increased from 80 to 300 points, and 170 points is found to give acceptable results. It is interesting to note that in the SPM case we needed 80 points as BMIA bandwidth that corresponded to $20l$ with the corresponding sampling, while in this case, the bandwidth is still in this scale, since it corresponds to $15l$. As we has assumed in the Section 4.2.1, the BMIA bandwidth appears to be related to the correlation length.

The study of convergence leads then to the following choice of parameters for the MOM solution of exponential rough surface in the PO range:

length of the profile	number of unknowns	window parameter g	BMIA bandwidth b
$80\lambda / 60l$	10 per λ	$\frac{L}{4}$	$15l$

Table 4.2.8. Parameters used for numerical simulations for exponential case.

Study of convergence $f=3\text{GHz}$ $kl=8.29$ $k\sigma=0.62$ $\epsilon_2=(3,0.1)$

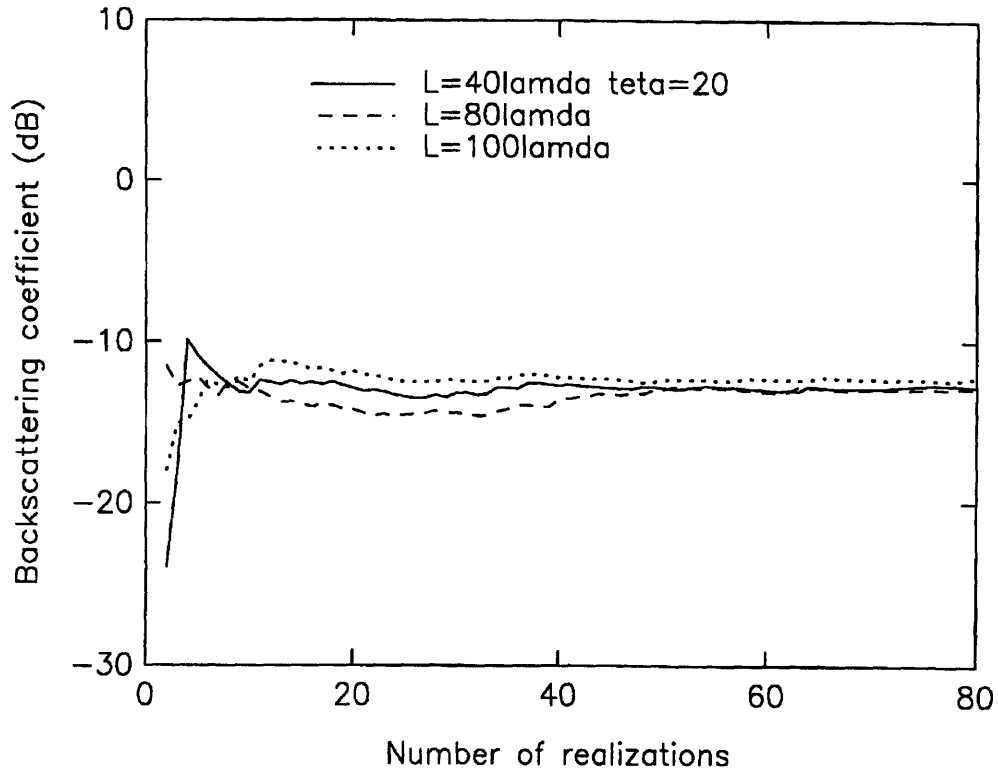


Figure 4.13. TE case: Study of convergence as a function of the length of the profile and the number of realizations for an exponential profile of $kl=8.29$, $k\sigma=0.62$, and $\epsilon_2=(3,0.1)$.

Study of convergence $f=3\text{GHz}$ $kl=8.29$ $ks=0.62$ $\epsilon_s=(3,0.1)$

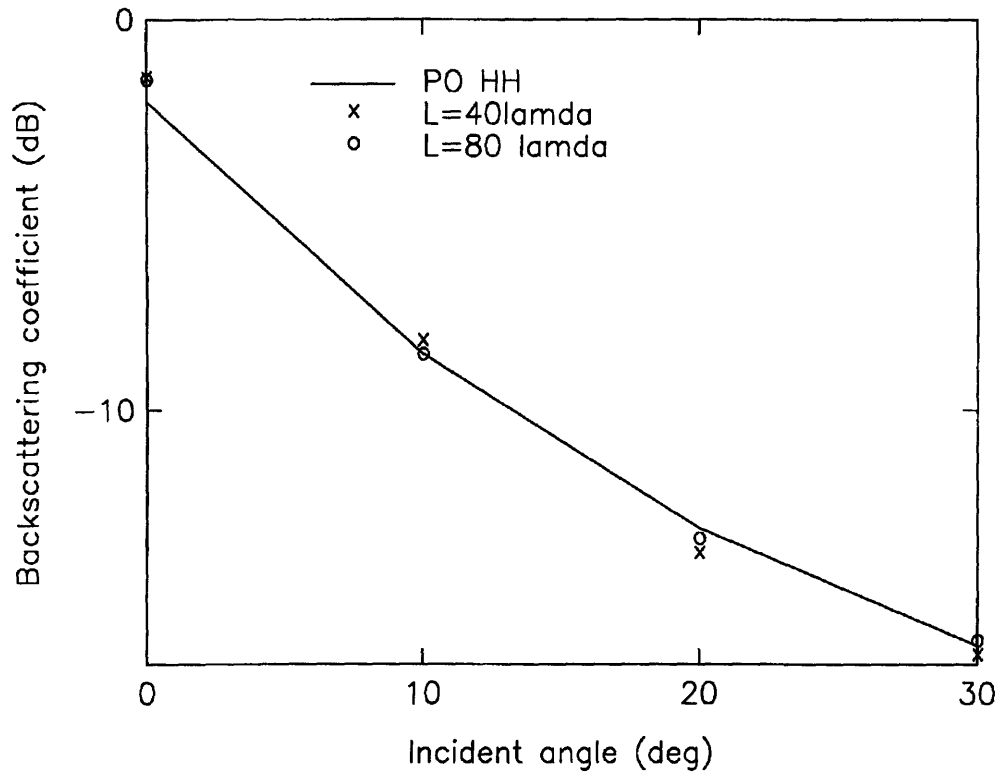


Figure 4.14. TE case: Study of convergence for $L=40\lambda$ and $L=80\lambda$ for an exponential profile of $kl=8.29$, $k\sigma=0.62$, and $\epsilon_2=(3,0.1)$.

The one-dimensional analytical PO results are calculated using the following estimated of the correlation length and rms height,

$\hat{\sigma}$	1.03 <i>cm</i>
\hat{l}	13.2 <i>cm</i>

Table 4.2.9. Estimated surface statistical parameters.

In Figure 4.15, the MOM results based on the parameters of Table 4.2.6 are plotted and compared with the analytical PO results obtained using the estimated statistical parameters of Table 4.2.7. Table 4.2.8 summarized the numerical results and the analytical PO results. The numerical and PO results of the backscattering coefficients are consistent within 0.2 dB difference , for all angles considered except at the zero degree incidence angle.

Incident Angle	Numerical results	Analytical results
0	-1.50	-2.11
10	-8.52	-8.56
20	-13.24	-13.02
30	-15.84	-16.02

Table 4.2.10. TE backscattering coefficients of the MOM and the analytical PO method for the exponential correlation function case.

A similar sensitivity study is also made for profiles with Gaussian correlation function. The study of convergence leads then to the following choice of parameters for the MOM solution of Gaussian random rough surfaces in the PO range:

Validation $f=3\text{GHz}$ $kl=8.29$ $ks=0.62$ $\text{eps}=(3,.1)$ expo.

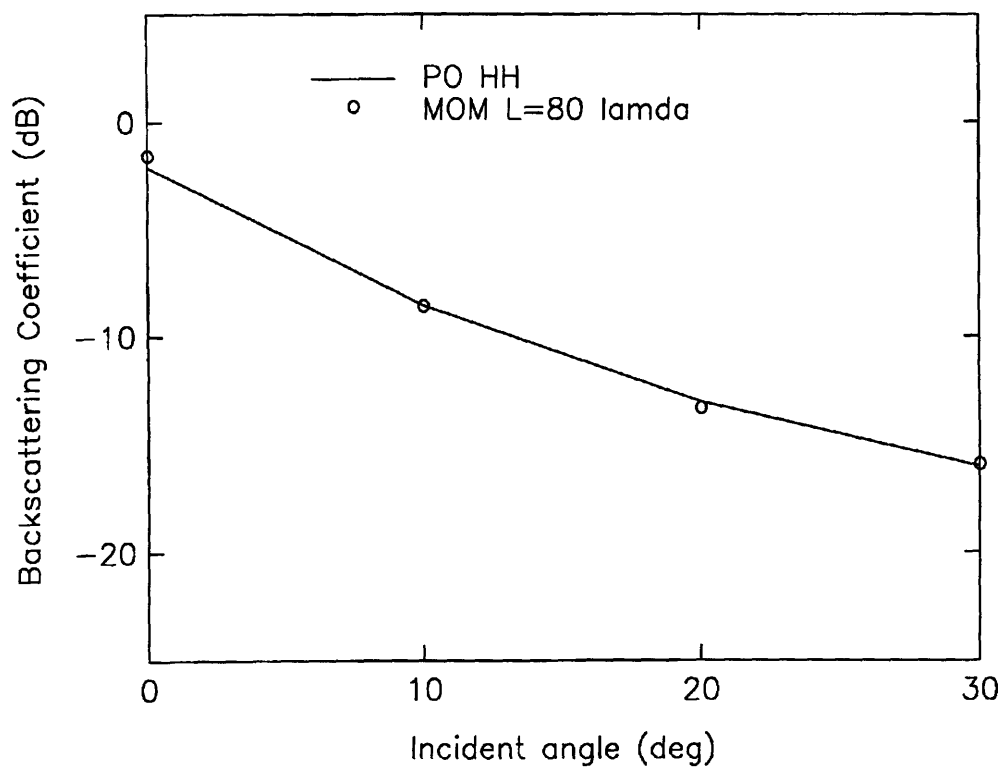


Figure 4.15. TE case: Comparison between MOM results and Physical Optics Model for an exponential profile of $kl=8.29$, $k\sigma=0.62$, and $\epsilon_2=(3,0.1)$.

length of the profile	number of unknowns	window parameter g	BMIA bandwidth b
$40 \lambda / 30 l$	10 per λ	$\frac{L}{4}$	20l

Table 4.2.11. Parameters used for numerical simulations for Gaussian case.

The one-dimensional analytical PO results were calculated using estimated values of the correlation length and rms height, computed from (4.4) and (4.6).

$\hat{\sigma}$	1.03 cm
\hat{l}	13.2 cm

Table 4.2.12. Estimated surface statistical parameters.

In the following table and Figure 4.16, the numerical results based on the parameters in Table 4.2.11 and analytical PO results based on the Table 4.2.12 are listed and compared.

Incident Angle	Numerical results	Analytical results
0	-1.78	-1.78
10	-7.40	-7.82
20	-18.56	-18.69
30	-32.10	-32.04

Table 4.2.13. TE backscattering coefficients of the MOM and the PO analytical method for the Gaussian case.

Validation $f=3\text{GHz}$ $kl=8.29$ $k\sigma=0.62$ $\epsilon_s=(3,.1)$ gauss.

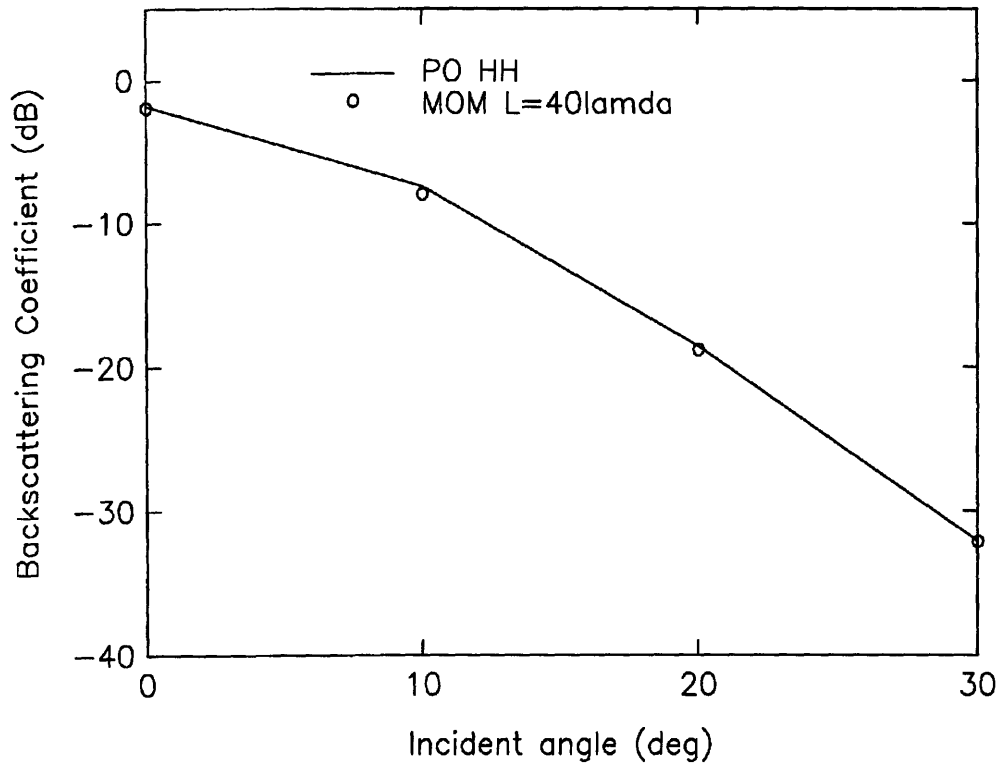


Figure 4.16. TE case: Comparison between MOM results and Physical Optics model for a Gaussian profile of $kl=8.29$, $k\sigma=0.62$, and $\epsilon_2=(3,0.1)$.

The numerical results match the P O results within 0.4 dB difference for the whole range of incidence angles considered. Similar studies are also performed with the TM case, and leads to the same numerical parameters as for the TE case. In the PO range, similar to the SPM case, both TE and TM case yield same conclusions, namely a longer length for the exponential profile is needed to reach the same criteria of convergence, and the same parameters lead to the same level of convergence.

When the dielectric constant of the profile is increased to $\epsilon_2 = (9,1)$, no difference on the required numerical parameters are observed, as can be seen on Figures 4.17 and 4.18. For the choice of numerical parameters in Tables 4.2.8 and 4.2.11, the backscattering coefficients predicted by MOM and PO match within 0.3 dB difference for all angles considered, and both for Gaussian and exponential cases.

This shows that when statistical parameters are identical, the numerical requirements for a Gaussian or an exponential profile are different in the PO range. As recalled from the discussion of Section 4.2.1, the correlation length considered now being equal to 1.23λ , the wavelength used now can see the difference between a Gaussian and an exponential profile in the short-range. This short-wavelength roughness, which characterized the exponential profile, asks for longer samples in the numerical computation in order to reach the required convergence criterion. Similar to the case of smoother surfaces, these requirements do not depend on either the wave polarization or the relative dielectric constants of the surfaces.

In the following section, very rough profiles with rms height large compared with the wavelength are considered.

4.2.3. Geometrical Optics Approximation

The Geometrical Optics model applies to the case of high frequency measurement or very rough surfaces, whose rms height is much larger than the wavelength. We will

Validation $f=3\text{GHz}$ $kl=8.29$ $ks=0.62$ $\text{eps}=(9,1)$ gaus.

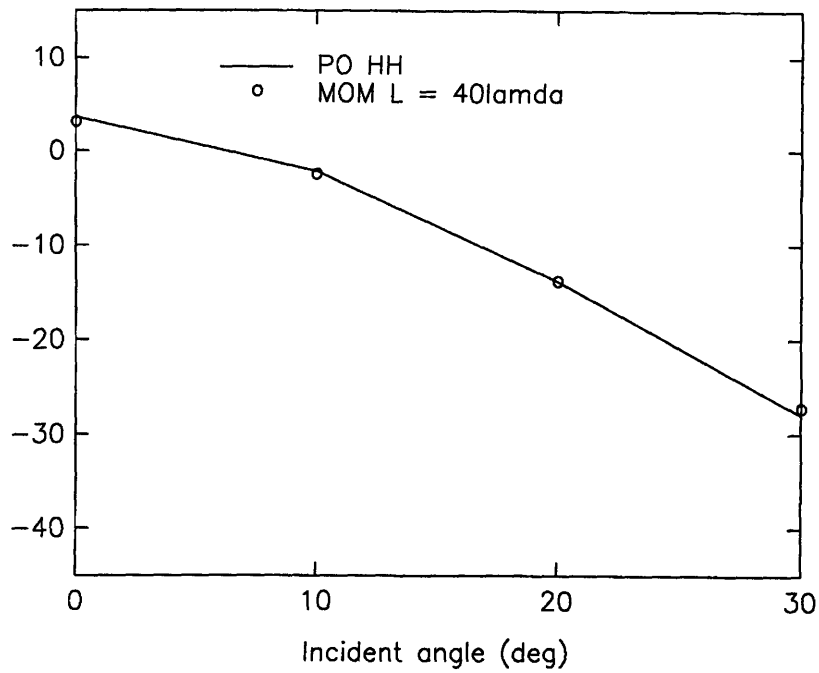


Figure 4.17. TE case: Comparison between MOM results and Physical Optics model for a Gaussian profile of $kl=8.29$, $k\sigma=0.62$, and $\epsilon_2=(9,1)$.

Validation $f=3\text{GHz}$ $kl=8.29$ $ks=0.62$ $\text{eps}=(9,1)$ expo.

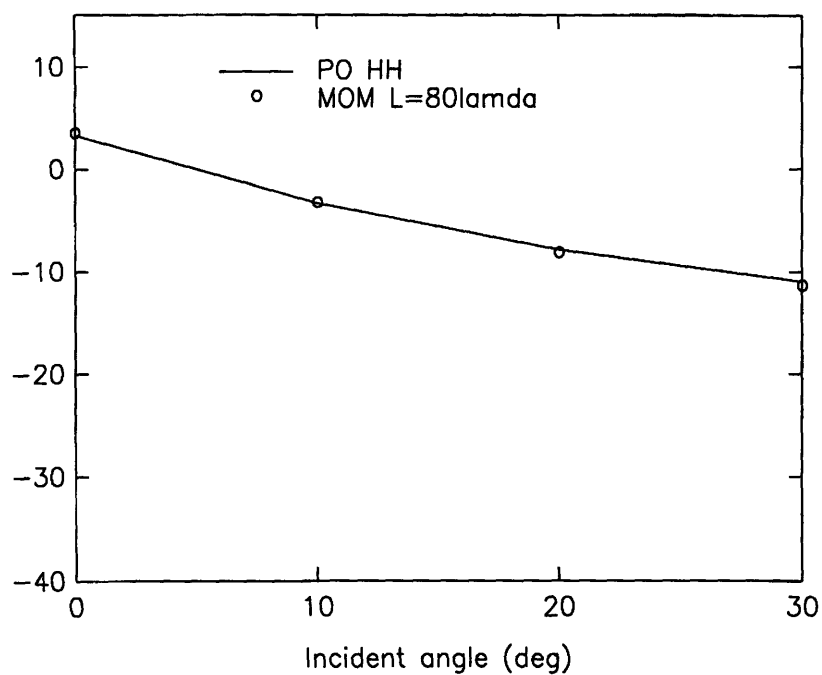


Figure 4.18. TE case: Comparison between MOM results and Physical Optics model for an exponential profile of $kl=8.29$, $k\sigma=0.62$, and $\epsilon_2=(9,1)$.

consider the following parameters that are in the domain of validity of this model as stated in Section 3.3

frequency	<i>9.5GHz</i>
Correlation function	Gaussian
<i>l</i>	<i>9cm</i>
σ	<i>3cm</i>

Table 4.2.14. Frequency and statistical parameters of the profile.

In this case we use the nominal parameters l and σ for the GO calculations. Indeed, the backscattering results obtained under GO approximation by using the estimated statistical parameters or the nominal ones show no more than 0.05 dB difference.

The same study as in the SPM and PO cases is performed. The length of the profile is increased from 40λ to 120λ . The simulations for profile length less than 100λ lead to divergent results with whatever the number of unknowns chosen. It may be explained if we express this profile length in term of the correlation length. In this case, 40λ corresponds to only $14l$ that is not long enough to capture the variability of the profile and its long-range correlation. The results for 100λ and 120λ are found to be within the 0.5 dB convergence criterion, after averaged over 160 realizations. In this case, where the surface profile is very rough, we need up to 160 realizations to reach the desired convergence of 0.5 dB for all angles considered. The actual difference is, in fact, less than 0.2 dB for angles except the zero degree incidence angle. A minimum length of 100λ appears then to be satisfying.

The BMIA bandwidth is increased from 70 pts to 300 pts. A value of $11l$ is found to give satisfactory results. The BMIA bandwidth b , as in the SPM and PO case, is within the interval of $[10l, 15l]$. It is logical that the longer the correlation length of a profile, the

larger is this parameter. Indeed, from the description of the BMIA method presented in Section 2.3, we recall that b is the half-bandwidth of the strong Matrix $\bar{\bar{Z}}^s$ which contains the elements within a band centered around the diagonal. Spatially, this decomposition means that we consider only in this matrix the interactions of neighboring points. Hence, when the correlation length is longer we must consider more interactions, and then larger BMIA bandwidth b .

The study of convergence leads then to the following choice of parameters for the MOM solution of Gaussian rough surface in the GO range:

length of the profile	number of unknowns	window parameter g	bandwidth b
$100\lambda / 35l$	1000/ 10 per λ	$\frac{L}{4}$	11l

Table 4.2.15. Parameters used for the numerical simulations for the Gaussian case.

In Figure 4.19, the MOM results based on the parameters of Table 4.2.15 are plotted and compared with the analytical GO results obtained using the nominal statistical parameters of Table 4.2.14. Table 4.2.16 summarized the numerical results and the analytical GO results.

Incident Angle	Numerical results	Analytical results
0	-6.60	-7.18
10	-7.00	-7.28
20	-7.79	-7.66
30	-8.59	-8.56

Table 4.2.16. TE backscattering coefficients of the MOM and the analytical GO method for the Gaussian case.

Validation $f=3\text{GHz}$ $kl=17.9$ $ks=5.96$ $\epsilon_s=(3,.1)$ gaus.

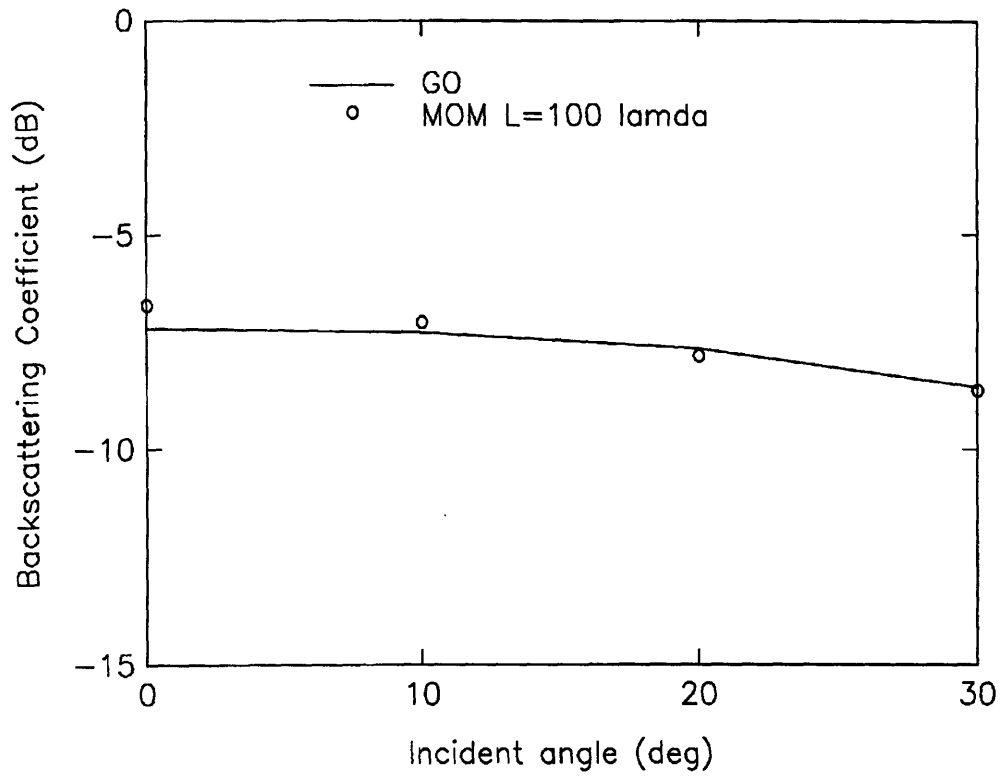


Figure 4.19. Comparison between MOM results and Geometrical Optics model for a Gaussian profile of $kl=17.9$, $k\sigma=5.95$, and $\epsilon_2=(3,0.1)$.

In Figure 4.19, we note that the values differ within 0.6 dB, in the whole range of incident angles considered.

It is worthwhile to note that the minimum profile length needed is longer in terms of wavelength than for the PO and SPM cases. But if expressed in term of correlation length, this minimum profile length is still in the range of $30/60l$. The correlation length appears then clearly to be the factor to use to fix the profile length required for convergence of the Method of Moments. Similar to the case of SPM and PO cases, these numerical requirements do not depend on either the wave polarization or the relative dielectric constants of the surfaces.

Chapter 5

Summary

The purpose of this study is to investigate the necessary numerical requirements when applying Method of Moments to solve the problem of electromagnetic wave scattering by a random rough penetrable surface. One-scale profiles with Gaussian or exponential correlation function are considered, and their numerical requirements compared.

In the first part, we present the direct or indirect classical methods of measurement of soil moisture before the development of radar, and underlined the advantages of active remote sensing. The remote sensing method can process large areas such as agricultural fields, often. A review of the classical and more recent analytical models developed in the past is also given.

In the second part the problem of a electromagnetic wave impinging on a one-dimensional penetrable rough surface is studied and solved with the Method of Moments. This method leads to a matrix equation that is solved numerically using a fast algorithm called Banded Matrix Iterative Approach.

Three different analytical models Small Perturbation Method, Physical Optics approximation and Geometrical Optics approximation are presented in the third part. These three analytical models are based on three different hypothesis of the roughness of the surface, leading to three different domain of validity.

In the last part, Monte-Carlo simulations are performed to compute numerically the HH and VV backscattering coefficients using the MOM. Surface profiles with three different roughness are studied corresponding to the three domains of validity of the analytical models. In each domain, two types of correlation functions, Gaussian and exponential, and two different dielectric constants are considered. A study of convergence is performed for each case in terms of the numerical parameters: length of the profile, number of unknowns, windowing parameter g , and b the bandwidth of the BMIA. The results are validated to be within 0.5 dB difference compared to the analytical results in all three cases for the range of incidence angles considered, 0 to 30 degrees. This precision is of 0.2 dB if we exclude the normal incidence case.

The numerical parameters required to reach such a convergence criterion appear to be independent on either the polarization or the relative dielectric constant. The length of the profile required depends on the roughness of the profiles. Hence, when the product of correlation length and wavenumber is increased, we need to use longer profiles measured in wavelengths to perform the numerical simulations. However, in terms of the scale of correlation length, these profiles all are in the range 30 to 60 times of their correlation length, depending on the autocorrelation function. Hence, for the Gaussian case, a profile length around $30l$ is satisfactory both in PO and GO range. The fact that the minimum profile length to reach the convergence criterion increases with the correlation length is logical, since the correlation length characterizes the correlation between remote points. The longer the correlation length is, the longer the profile length considered must be to capture this statistic. We must therefore consider not only the wavelength, as it is commonly done, but also the correlation length when applying the Method of Moments.

The minimum profile length depends also on the autocorrelation function considered, when the profile correlation length is long enough compared to the wavelength. Hence, in the PO range, a profile as long as $60l$, twice as long as for the Gaussian case, is required

for the exponential case. But in the SPM range, the profile lengths are equal. These results are consistent with the intuitive perceptions we had when observing two profiles as in Figures 4.1.a and 4.1.b. The exponential profiles can be seen as the superposition of a Gaussian surface in the long-range while with short-wave-length roughness. When the correlation increases in term of wavelength, the electrical field is able to see this short-range fluctuation, and Gaussian and exponential profiles become differentiable. In the SPM case, the electromagnetic wave is unable to "see" such a difference at a scale less than its own wavelength. Hence the HH backscattering coefficients in the SPM range are found to be in the same range at 2 dB for all angles considered. But in the PO range, the correlation length is now of the order of the wavelength, and the differences between HH backscattering coefficients for the Gaussian and exponential case are then as large as 15 dB at a 30 degree incidence angle. In the SPM case, the difference between Gaussian and exponential profiles were however marked by the number of realizations required to reach the convergence criterion. Hence, we observe that in the SPM domain of validity, exponential profiles require more realizations than Gaussian profiles to reach the desired level of convergence.

The number of unknowns, 10 points per wavelength, is satisfactory for all profiles. The windowing parameter g gives convergent results when sets equal to $L/4$ in all cases.

The BMIA bandwidth b is found to be within $11l$ and $15l$, whatever the roughness, or the correlation function. This dependence on the correlation length l is logical when we recall the spatial meaning of this numerical parameter. Spatially, the strong matrix in the BMIA method take into account only the interactions of neighboring points. Hence, when the correlation length is large, i.e. remote points are correlated, we must consider more neighboring interactions, and then increase the BMIA bandwidth b .

Appendix

Under the Physical Optics approximation, the backscattering coefficient for one-dimensional rough surface is, as stated in Chapter 3,

$$\sigma_{pp}^o = \sigma_{inc,pp}^o + \sigma_{slope,pp}^o \quad (\text{A.1})$$

where

$$\sigma_{inc,pp}^o = 2k_1 |R_{pp}|^2 \cos^2 \theta_i \exp(-K_o) \sum_{n=1}^{\infty} \frac{(K_o)^n}{n!} \left(\int_0^{+\infty} C^n(u) \cos(q_x u) du \right) \quad (\text{A.2})$$

and

$$\begin{aligned} \sigma_{slope,pp}^o = & i2k_1 q_z \sigma^2 \left[|R_{pp}|^2 \sin \theta_i \cos \theta_i + \Re(R_{pp} R_{pp1}^*) \cos^2 \theta_i \right] \\ & \times \exp(-K_o) \sum_{n=0}^{\infty} \frac{(K_o)^n}{n!} \left(\int_0^{+\infty} \frac{dC}{du} C^n(u) \cos(q_x u) du \right) \end{aligned} \quad (\text{A.3})$$

For one-scale profiles with either exponential or Gaussian autocorrelation function, we find

$$I_0 = \int_{-\infty}^{+\infty} C^n(u) \exp(q_x u) du = \frac{2nl}{n^2 + (q_x l)^2} \text{ for exponential case} \quad (\text{A.4})$$

$$I_0 = \int_{-\infty}^{+\infty} C^n(u) \exp(q_x u) du = \frac{l\sqrt{\pi}}{\sqrt{n}} \exp\left(\frac{-(q_x l)^2}{4n}\right) \text{ for Gaussian case} \quad (\text{A.5})$$

$$I_1 = \int_{-\infty}^{+\infty} \frac{dC}{du} C^n(u) \exp(q_x u) du = \frac{-2iq_x l}{(q_x l)^2 + (n+1)^2} \text{ for exponential case} \quad (\text{A.6})$$

$$I_1 = \int_{-\infty}^{+\infty} \frac{dC}{du} C^n(u) \exp(q_x u) du = \frac{-iq_x l \sqrt{\pi}}{(n+1)^{3/2}} \exp\left(-\frac{(q_x l)^2}{4(n+1)^2}\right) \text{ for Gaussian case} \quad (\text{A.7})$$

Bibliography

- [1] Bass F., and Fucks I.M., "Wave Scattering from Statistically Rough Surfaces," Pergamon, pp. 525, New York, 1979.
- [2] Kong J. A., *Electromagnetic Wave Theory*, Second Edition, Wiley, New York, 1990.
- [3] Ulaby F.T., R.K. Moore, and A.K. Fung, *Microwave remote sensing active and passive*, vol. 2, Addison-Wesley, 1982.
- [4] Wilson R.G., "Methods of measuring soil moisture : National Research Council, International Year for the Great Lakes," *Technical Manual Series*, vol. 1, 1970.
- [5] Nutting P.G., "Some standard thermal dehydration curves of minerals," *U.S Geol. Survey*, Prof. Paper 197E., 1943.
- [6] Black C.A., "Methods of soil analysis. Part I. Physical and mineralogical properties," *Agronomy*, vol. 9, pp. 89-125, American Society of Agronomy, Inc., Publisher, 1965.
- [7] Belcher D.J., T.R. Cuykendall and H.S. Sack, "The measurement of soil moisture and density by neutron and gamma-ray scattering," *Civil Aeron. Tech. Develop.*, Rpt. n° 127, 1950.
- [8] Collet L.S., "Advances in Surface Geophysical Techniques for Ground Water and Soil Moisture," *Remote sensing of soil moisture and ground water*, pp. 51-63, Toronto, 1976.
- [9] Skolnik M.I., *Introduction to radar systems*, McGraw-Hill Book Company, 1980.
- [10] Ulaby F.T., J. Cihlar, and R.K. Moore, "Active microwave measurement of soil water content," *Remote sensing of Env.*, vol. 3, pp. 185-203, 1974.
- [11] De Loor G.P., "Dielectric properties of heterogeneous mixtures," Ph-D Thesis, University of Leiden, Netherlands, 1956.
- [12] Hoeckstra P. and A. Delaney, "Dielectric properties of soils at UHF and microwaves frequencies," *J. Geophys. Res.*, 79, pp. 1699-1708, 1974.

- [13] Dobson M.C. and F.T. Ulaby, "Active microwave soil moisture research," *I.E.E.E. Trans. Geosci. Remote Sensing*, vol. GE-24, pp. 23-26, Jan. 1986.
- [14] Hallikainen M.T. et al., "Microwave dielectric behavior of wet soil: Empirical models and observations," *I.E.E.E. Trans. Geosci. Remote Sensing*, vol. GE-23, n°1, pp. 25-46, Jan. 1985.
- [15] Shin R.T. and J.A. Kong, "Scattering of electromagnetic waves from a randomly rough perturbed quasi-periodic surface," *J. Appl. Phys.*, vol. 56, 1984.
- [16] Church E.L., "Fractal surface finish," *Applied Optics*, vol. 27, pp. 1518-1526, 1988.
- [17] Keller J.M. et al., "Characteristics of natural scenes related to the fractal dimension," *I.E.E.E. Trans. Pattern. Anal. Machine Intell.*, PAMI-9(5), pp. 621-627, 1987.
- [18] Manninen A.T., "Surface roughness of Baltic sea ice," *Journal of Geophys. Res., Oceans*, 1996.
- [19] Elson J.M. et al., "Light scattering from multi-layer optics: comparison of theory and experiment," *Applied Optics*, vol. 19, pp. 669-679, 1980.
- [20] Prusinkiewicz P. and A. Lindenmayer, "Fractal properties of plants, the algorithm beauty of plants," Springer-Verlag, 1990.
- [21] Ogilvy J.A. "Theory of wave scattering from random rough surfaces," published by IOP publishing Ltd., Institute of Physics publishing, Bristol and Philadelphia, 1991.
- [22] Le Mehaute A., *Les geometries fractales*, Hermes, 1990.
- [23] Keller J.M. et al., "Texture description and segmentation through fractal geometry," *Computer vision, graphics and image processing*, vol. 45, n° 2, pp. 150-166, 1989.
- [24] Jaggard D.L., "On fractal electrodynamics, recent advances in electromagnetic theory," Springer-Verlag, pp. 183-222, 1990.
- [25] Rice S.O., "Reflection of electromagnetic waves from slightly rough surfaces," *Commun. pure Appl. Math.*, vol. 4, pp. 351-378, 1951.
- [26] Valenzuela G., "Depolarization of EM waves by slightly rough surfaces," *I.E.E.E. Trans. Antennas Propag.*, vol. 15, n° 4, pp. 552-557, 1967.
- [27] Ishimaru A. and J.S. Chen, "Scattering from very rough surfaces based on the modified second order Kirchhoff approximation with angular and propagation shadowing," *J. Acoust. Soc. Am.*, vol. 88, pp. 1877-1883, 1990.
- [28] Brown G.S., "Backscattering from a Gaussian distributed, perfectly conducting rough surface," *I.E.E.E. Trans. Antennas Propag.*, AP-26, pp. 472-482, 1978.

- [29] Mc Daniel S.T. and A.D. Gordman, "An examination of the composite-roughness scattering model," *J. Acoust. Soc. Am.*, vol. 73, pp. 1476-1486, 1983.
- [30] Shen J. and A. A. Maradudin, "Multiple scattering of waves from random rough surfaces," *Phys. Rev. B. Condens. Matter*, vol. 22, pp. 4234-4240, 1980.
- [31] Winebrenner D.P. and A. Ishimaru, "Investigation of a surface field phase perturbation technique for scattering from rough surfaces," *Radio Sci.*, vol. 20, pp. 161-170, 1985.
- [32] Winebrenner D.P. and A. Ishimaru, "Application of the phase perturbation technique to randomly rough surfaces," *J. Opt. Soc. Am. A.*, vol. 2, pp. 2285-2293, 1985.
- [33] Rodriguez E., "Beyond the Kirchhoff approximation," *Radio Sci.*, vol. 24, pp. 681-693, 1989.
- [34] Rodriguez E., "Beyond the Kirchhoff approximation II, electromagnetic scattering," *Radio Sci.*, vol. 26, pp. 121-132, 1991.
- [35] Bahar E., "Scattering cross sections for composite random surfaces: Full wave analysis," *Radio Sci.*, vol. 16, pp. 1327-1335, 1981.
- [36] Holliday D., "Resolution of a controversy surrounding the Kirchhoff approach, and small perturbation method in rough surface scattering theory," *I.E.E.E Trans. Antenna Propag.*, AP-35, pp. 120-122, 1987.
- [37] Fung A.K. et al., "Backscattering from a randomly rough dielectric surface," *I.E.E.E Trans. Geosci. Remote Sensing*, vol. 30, pp. 356-369, 1992.
- [38] Fung A.K. et al., "A further study of the IEM surface scattering model," *Proceedings IGARSS' 96*, pp. 2116-2118, Lincoln, Nebraska, 1996.
- [39] Harrington R.F., *Field computations by moment methods*, Mac-Millan Company, New-York, 1968.
- [40] Yee K.S., "Numerical Solution of Initial Boundary Value Problems Involving Maxwell's Equations in Isotropic Media," *I.E.E.E Trans. Antenna Propag.*, vol. 14, n° 3, pp. 302-307, 1996.
- [41] *11th Annual review of progress in Applied Computational Electromagnetics*, Proceedings, Applied Computational Electromagnetics Society, 1995.
- [42] Axline R.M. and A.K. Fung, "Numerical computation of scattering from a perfectly conducting random surface," *I.E.E.E Trans. Antenna Propag.*, AP-26, pp. 482-488, 1978.
- [43] Fung A.K and M.F. Chen, "Numerical simulation of scattering from simple and composite random surfaces," *J. Opt. Soc. Am. A.*, vol. 2, pp. 2274-2284, 1985.

- [44] Chen M.F. and A.K. Fung, "A numerical study of the regions of validity of the Kirchhoff and small-perturbation rough surface scattering models," *Radio Sci.*, vol. 23, pp. 163-170, 1988.
- [45] Durden S.L. and J.F. Vesecky, "A numerical study of the separation wave number in the two-scale scattering approximation," *I.E.E.E. Trans. Geosci. Remote Sensing*, vol. 28, pp. 271-272, 1990.
- [46] Thorsos E.I., "The validity of the Kirchhoff approximation for rough surface scattering using a Gaussian roughness spectrum," *J. Acoust. Soc. Am.*, vol. 83, pp. 78-92, 1988.
- [47] Thorsos E.I. and D.R. Jackson, "The validity of the perturbation approximation for rough surface scattering using a Gaussian roughness spectrum," *J. Acoust. Soc. Am.*, vol. 86, pp. 261-277, 1989.
- [48] Soto-Crespo J.M. et al., "Scattering from slightly rough random surfaces: A detailed study of the validity of the small perturbation method," *J. Opt. Soc. Am. A.*, vol. 7, pp. 1185-1201, 1990.
- [49] Sanchez-Gil J.M. and M. Nieto-Vesperinas, "Light scattering from random rough dielectric surfaces," *J. Opt. Soc. Am. A.*, vol. 8, pp. 1270-1286, 1990.
- [50] Broschat S.L. et al., "The phase perturbation technique versus an exact numerical method for random rough surface scattering," *J. Electromagn. Waves Appl.*, vol. 3, pp. 237-256, 1989.
- [51] Rodriguez E. et al., "A numerical assessment of rough surface scattering theories: Horizontal polarization," *Radio Sci.*, vol. 27, pp. 497-513, 1992.
- [52] Press W.H., S.A. Teukolsky, W.T. Vetterling, and B.P. Flannery, *Numerical Recipes: the Art of Scientific Computing*, second edition, Cambridge Univ. Press., New-York, 1992.
- [53] Barret R., M. Berry, T. Chan, J. Demmel, J. Donato, J. Dongarra, V. Eijkhout, R. Pozo, C. Romine, and H. van der Vorst, *Templates for the Solution of Linear Systems: Building Blocks for Iterative Methods*, available by ftp from netlib.cs.utk.edu, 1993.
- [54] Tsang L. et al., "Monte-Carlo simulations of large scale composite random rough surface scattering based on the banded matrix iterative approach," *J. Opt. Soc. Am.*, vol. 11, pp. 1153-1154, 1993.
- [55] Tsang L. et al., "Monte-Carlo simulations of a two dimensional random rough surface using the sparse matrix flat surface iterative approach," *Electronics Letter*, vol. 29, pp. 1153-1154, 1993.
- [56] Johnson J.T., "Applications of numerical methods for rough surface scattering," Ph.D. Thesis, Massachusetts Institute of Technology, Cambridge, USA, 1996.

- [57] Fung A.K. and H.J. Eom, "Note on the Kirchhoff rough surface solution in backscattering," *Radio Science*, vol. 3, pp. 299-302, 1981.
- [58] Chuang S. and J.A. Kong, "Scattering of waves from periodic surfaces," *Proc. I.E.E.E.*, vol. 69, pp. 1132-1144, 1981.
- [59] Mc. Cammon D.F. and S.T. Daniel, "Application of a new theoretical treatment to an old problem: sinusoidal pressure release boundary scattering," *J. Acoust. Soc. Am.*, vol. 78, pp. 149-156, 1985.
- [60] Zaki K.A. and A.R. Neurether, "Scattering from perfectly conducting surface with a sinusoidal height profile: TE polarization," *I.E.E.E Trans. Antenna Propag.*, AP-19, pp. 208-214, 1971.
- [61] Chan H.L. and A.K. Fung, "A Numerical Study of the Kirchhoff Approximation in horizontally polarized backscattering from a random surface," *Radio Sci.*, vol. 13, pp. 811-818, 1978.
- [62] Li L. et al., "Numerical simulation of conical diffraction of tapered electromagnetic waves from random rough surfaces and applications to passive remote sensing," *Radio Sci.*, vol. 29, n° 3, pp. 587-598, 1994.
- [63] Ishimaru A., *Electromagnetic Wave Propagation, Radiation, and Scattering*, Prentice Hall, pp. 153, N.J., 1991.
- [64] Chan C.H et al., "A Banded Matrix Approach to Monte-Carlo Simulations of Large-Scale Random Rough Surface Scattering: Penetrable Case", *Ninth Annual Review of Progress in Applied Electromagnetic*, Conference Proceedings, pp. 391-397, 1993.
- [65] Ogilvy J.A., and J.R Foster, "Rough Surfaces: Gaussian or exponential statistics?," *J. Physics D: Appl. Physics*, vol. 22, pp. 1243-1251, 1989.
- [66] Ogilvy J.A., "Computer simulation of acoustic wave scattering from rough surfaces," *J. Physics D: Appl. Physics*, vol. 21, pp. 260-277, 1988.